Investigation of Dynamic Ultrasound Reception in Bat Biosonar Using a Biomimetic Pinna Model

Mittu Pannala

Dissertation submitted to the Faculty of the
Virginia Polytechnic Institute and State University
in partial fulfillment of the requirements for the degree of

Doctor of Philosophy
in
Mechanical Engineering

Rolf Müller, Chair
Javid Bayandor
Alexander Leonessa
Shashank Priya
John Socha

November 1, 2013
Blacksburg, Virginia

Keywords: bat biosonar, pinna deformation, biomimetic model,
dynamic sensing, sensory coding capacity

Investigation of Dynamic Ultrasound Reception in Bat Biosonar Using a Biomimetic Pinna Model

Mittu Pannala

ABSTRACT

Bats are a paragon of evolutionary success. They rely on parsimonious sensory inputs provided by echolocation, yet are able to master lives in complex environments. The outer ears (pinnae) of bats are intricately shaped receiver baffles that encode sensory information through a diffraction process. In some bat species with particularly sophisticated biosonar systems, such as horseshoe bats (Rhinolophidae), the pinnae are characterized by static as well as dynamic geometrical features. Furthermore, bats from these species can deform their pinnae while the returning ultrasonic waves impinge on them. Hence, these dynamic pinna geometries could be a substrate for novel, dynamic sensory encoding paradigms.

In this dissertation, two aspects of this dynamic sensing process were investigated: (i) Do local shape features impact the acoustic effects during dynamic deformation of the bat pinna? and (ii) do these shape deformations provide a substrate for the dynamic encoding of sensory information? For this, a family of simplified biomimetic prototypes has been designed based on obliquely truncated cones manufactured from sheets of isobutyl rubber. These prototypes were augmented with biomimetic local shape features as well as with a parsimonious deformation mechanism based on a single linear actuator. An automated setup for the acoustic characterization of the time-variant prototype shapes has been devised and used to characterize the acoustic responses of the prototypes as a function of direction.

It was found that the effects of local shape features did interact with each other and with the deformation of the overall shape. The impact of the local features was larger for bent than for upright shape configurations. Although the tested devices were much simpler than actual bat pinnae, they were able to reproduce numerical beampattern predictions that have been obtained for deforming horseshoe bat pinnae in a qualitative fashion.

The dynamically deformable biomimetic pinna shapes were estimated to increase the sensory encoding capacity of the device by 80 % information when compared to static baffles. To arrive at this estimate, spectral clustering was used to break up the direction- and deformation-depended device transfer function into a discrete signal alphabet. For this alphabet, we could estimate the joint signal entropy across a bending cycle as a measure for sensory coding capacity.

The results presented in this thesis suggest that bat biosonar posses unique dynamic sensing abilities which have no equivalent in man-made technologies. Sensing paradigms derived from bat biosonar could hence inspire new deformable wave-diffracting structures for the advancement in sensor technology.

GRANT INFORMATION

This work was supported by grants from the National Aeronautics and Space Administration, the US Army Research Office, and the National Science Foundation.

Dedication

This dissertation is dedicated to

my Mom - Bokka Satyavati - for her unconditional love and support

and

my Dad - Pannala Ramachandra Reddy - for, he is my role model

I love you Mummy and Daddy

Acknowledgments

I would first and foremost thank my committee chairperson, Dr. Rolf Mueller for his invaluable support and advice throughout the course of my graduate program. I have gained a great deal of research experience from working under Dr. Mueller. Words cannot express my gratitude for his support throughout my program.

I also thank my committee members, Dr. Javid Bayandor, Dr. Alexander Leonessa, Dr. Shashank Priya and Dr. Jake Socha for serving on my committee. Thank you for your comments and suggestions and appreciation of my work.

Next, I want to thank Dr. Naren Ramakrishnan and Dr. Hongxiao Zhu for their valuable input and help with information theoretic methods.

My next set of thanks goes to my lab-members: Anupam Gupta, Lvyin Cai, Philip Caspers, Uzair Gillani and Yanqing Fu for creating a great working environment.

My roommates, Atashi Sharma, Meeta Srivastav and Tina Nandy have helped create a home-away-from-home. Without you guys, it wouldn't have been as much fun.

I also want to thank Amanda Glenn, Cathy Hill, Pam Patterson and Robin Barker for their help with administrative work.

This next set of thankyou goes to a special set of people: Sarang Supekar, Rachit Sharma, Sravani Duggirala, Cameron Rainey, Mehran Motamedi, Sajjad Meymand, Harisha Pannala and Gautami Gowdelli for trusting and believing in me and always standing by my side.

I want to thank my new found love - Dr. Ravi Sekhar Tummidi :-)

Finally and most importantly, I want to thank my parents for their unconditional love, support and encouragement. You both are the reason I have been able to achieve, what I have today. I love you both very much.

Contents

1 Introduction **1**

1.1 Biosonar-inspired technology 1

1.2 Bat biosonar as a model 2

1.3 Sensor dynamics in horseshoe bats 4

1.4 Objective and Approach 9

1.5 Chapter outline 12

2 Biomimetic Prototype **13**

2.1 Simplified prototype: basic shape 13

2.2 Local shape features 15

2.3 Prototype fabrication 16

3 Experimental Characterization **20**

3.1 Actuation mechanism for the dynamic deformation of the prototype 20

3.2 Experimental setup 22

3.3 Time-variant signal processing 25

4 Local Shape Features **27**

4.1 Reproducibility 27

4.2 Plain cone behavior 28

4.3 Interplay between shape features 30

4.4 Quantitative analysis of the beampatterns 31

4.5 Biomimicry 36

4.6 Discussion 37

5 Dynamic Sensor Encoding **40**

5.1 Introduction 40

5.2 Information-theoretic analysis of biological systems 41

5.3 Coding capacity of the biomimetic pinnae 42

5.4 Spectral clustering 44

5.5 Sampling bias corrections 45

5.6 Permutation test 47

5.7 Results 47

5.8 Discussion 51

6 Summary **55**

6.1 Research accomplishments 55

6.2 Major findings 56

6.3 Suggestions for future work 57

Bibliography **60**

7 Appendix A **67**

8 Appendix B **69**

List of Figures

1.1 Examples of biosonar pulse sequences with synchronized measurements of the velocity of the anterior rim of the noseleaf in the proximal-distal direction: (a) example sequence with non-random motions of the anterior leaf. (b) example sequence without non-random motions. For each example, the top graph shows the envelope of the sound pressure amplitude, the center graph the velocity, and the bottom graph the displacement amplitude of the anterior rim of the noseleaf in the proximal-distal direction. Positive velocities and displacements correspond to motions in the distal direction (i.e., away from the head). Reproduced from [16]. See page 2 of copyright permissions document. 5

1.2 Some of the muscles in the outer ear of the greater horseshoe bat (*Rhinolophus ferrumequinum*). From [19], reproduced with permission. See page 3-8 of copyright permissions document. 7

1.3 Frames from a high-speed video-recording of the ear deformation of the horseshoe bat. 8

2.1 Fabrication of the basic prototype shape: (a) isobutyl rubber sheet, (b) leaf-shaped cutout, (c) cutout folded at one end, (d) trimmed to the final truncated cone shape. . 16

2.2 Eight plain cone prototypes manufactured for testing the reproducibility of the beampatterns and repeatability of the fabrication method. 17

2.3 Comparison of a horseshoe bat pinna with the simplified prototype: (a) local shape features extracted from the greater horseshoe bat, (b) plain cone augmented with the local features. 18

2.4 Set of prototypes augmented with biomimetic shape feature combinations: (a) no features, (b) ridge, (c) incision, (d) antitragus, (e) ridge and incision, (f) incision and antitragus, (g) ridge and antitragus, (h) ridge, incision, and antitragus. 19

3.1 Single point actuation mechanism of the biomimetic prototype: (a) front view, (b) side view. 21

3.2 Seven shape changes from upright to bent configuration in the ear prototype. 21

3.3 Actuation setup mounted on the Pantilt unit. 23

3.4 Experimental Setup: The ear prototype is placed at a far field region with respect to the loudspeaker. 24

3.5 Block diagram of the automated characterization setup. 25

3.6 Time-variant signal processing: (a) spatial direction of the recorded signals, (b) recorded signal at one particular position in the direction space, (c) amplitude spectrum after fast-Fourier transforming the signal and (d) beampatterns for frequencies obtained by combining the spectra. 26

4.1 Reproducibility of the results: Beampatterns obtained from the different realizations of the plain cone shape. Rows from bottom to top are patterns at frequencies of 24 kHz (corresponds to 60 kHz in bats) to 32 kHz (corresponds to 80 kHz in bats) at an interval of 2 kHz. The columns represent the plain cone prototypes. . . . 28

4.2 Beampatterns at various bending stages for plain cone shape. Rows represent the frequencies from 24 kHz for prototype (corresponds to 60 kHz in bats) to 32 kHz for prototype (corresponds to 80 kHz in bats) at an interval of 2 kHz. Columns represent bending stages from upright to bent. 29

4.3 Beampatterns at various bending stages for cone shapes augmented with individual shape features or feature combinations: Two frequencies, low (26 kHz for prototype corresponds to 65 kHz in bats) and high (30 kHz for prototype corresponds to 75 kHz in bats), are shown for each feature combination and bending stage. 31

4.4 Beampatterns at upright and bent stages for cone shapes augmented with individual shape features or feature combinations: Three frequencies, 24 kHz, 28 kHzand 32 kHz for prototype corresponds to 60 kHz, 70 kHz and 80 kHz in bats, are shown for each feature combination and bending stage. 32

4.5 Computation of the amplitude-weighted sidelobe number from the beam gain values. The maximum amplitudes (triangles) of the sidelobes (1, 2, 3) are summed. Beam gain values are coded in gray scale from white (low values) to gray (high values). White region below -30° was not covered by the measurement 33

4.6 Amplitude-weighted number of sidelobes along frequencies and deformation stages. In each set of eight bar figures, from left to right-ear with no features, ear with one feature (ridge, incision, antitragus), ear with combination of features. 34

4.7 Multiple population t-tests (with Bonferroni correction) on the shape groups based on amplitude-weighted number of sidelobes. 'Cone' population consists of only plain cone data, 'single feature' population consists of data from prototypes with one feature, 'multi feature' population consists of data from prototypes with more than one feature. 35

4.8 Elevation beamwidth along frequencies and deformation stages. In each set of eight bar figures, from left to right-ear with no features, ear with one feature (ridge, incision, antitragus), ear with combination of feature. 36

4.9 Multiple population t-tests (with Bonferroni correction) on the shape groups based on elevation beamwidth of the lobes. 'Cone' population consists of only plain cone data, 'single feature' population consists of data from prototypes with one feature, 'multi feature' population consists of data from prototypes with more than one feature. 37

4.10 Biomimetic prototype beampattern comparisons:(a) Screenshots from a high-speed video recording of the pinna deformation in the greater horseshoe bat, (b) numerical beampattern estimates of the pinna deformation, (c) biomimetic ear prototype at different shape deformations and (d) experimental beampattern estimates for the ear prototype. 38

5.1 Example transfer functions for four positions in the directivity space (linear scale) . 44

5.2 100 % variability found in 33 of the 129 dimensions. Only 50 dimensions are shown on the x-axis 45

5.3 Clustering of beampatterns of different bending stages into discrete alphabets based on spectral clustering applied to transfer function vectors. Columns indicate alphabet sizes of two (top) to ten (bottom). Color codes for the different elements of the alphabet. 48

5.4 Entropy estimates for the discretized beampatterns as a function of alphabet size. The different bars in the groups for each alphabet size represent the different bending states of the biomimetic device from upright (blue) to bent (red). The horizontal bar over each group indicates the maximum entropy that is possible for the respective alphabet size ($H_{\max} = \log_2 |A|$, where A is the alphabet size [53]). . . . 49

5.5 Mutual information reaches maximum and then decays to zero with increase in alphabet size. Up to 100 clusters are shown here. The colors represent different bending stages - red, blue, green, magenta, black and cyan in order indicate upright to bent stages. 50

5.6 Increase in encoding capacity over the bending sequence of the biomimetic prototype as normalized mutual information between the discretized beampattern of the upright baffle shape compared to successive bending stages decreases. 52

5.7 Increase in encoding capacity over the bending sequence of the biomimetic prototype: joint entropy across the different bending stages studied. Individual bars in the groups correspond to the different discrete alphabet sizes from two (blue) to ten (red). 53

6.1 Characterization in the time-direction domain: impulse response amplitude as a function of time in the deformation cycle (rows) and time delay (columns). Colored version of the figure reproduced from [40]. See page 10 of copyright permissions document. 58

6.2 Characterization in the delay-time domain. Colored version of the figure reproduced from [40]. See page 10 of copyright permissions document. 59

7.1 Gaussian distribution binned with bin numbers of 2, 10, 200, and 10,000. The continuous distribution is represented by the red line. 68

8.1 True mutual information evaluated from the permutation tests. 70

List of Tables

2.1 Overview of the analyzed set of biomimetic baffle prototypes. 19

Chapter 1

Introduction

1.1 Biosonar-inspired technology

Bioinspired science and technology is an interdisciplinary field of study at the intersection of biology and engineering. It seeks to understand the principles of biological function from an engineering perspective and use these insights in the design of technical devices. Engineers have been looking at biological systems as a source of inspiration for a long time already and the approach has produced significant advances in fields such as surface coating (e.g., self-cleaning Lotusan paint [1]), reversible adhesion (e.g., Velcro [2]), parsimonious sensing (e.g., motion sensor of the optical mouse [3]).

The performance of biological systems is often due to an integration of functional features across multiple levels and aspects of biological organization. Biological materials, for example, are often "metamaterials" with properties that result from structural features that range from the nano- and micro- all the way up to the macroscopic scale. Similarly, the function of many biological structures can only be understood from their behavioral, ecological, and evolutionary contexts. Hence, one of the central challenges for the future development of bioinspired science and technology is to find ways in which the principles of biological system integration can be understood and applied

to the design of engineered systems.

Bat biosonar has obvious parallels to technical sensing systems such as sonar and radar. However, in the past these technical systems have been used mainly in contexts that provide a poor match for the conditions under which bat biosonar systems operate. The radar system of a fighter airplane, for example, is operated at much higher speeds and needs to sense its environment on a much larger scale than the biosonar system of bats. Similarly, submarine sonar needs to operate on a much larger scale than bat biosonar. This situation has begun to change in recent years, as small autonomous vehicles have gained importance for operation in air as well as under water. Such systems, e.g., micro-air vehicles (MAVs), are often intended for use in small-scale, structure-rich environments that are not unlike those inhabited by bats. At present, a large performance gap continues to exist between the capabilities of bats in such environments and those that technical systems can achieve. Bats are able to traverse even dense vegetation at high speeds (over 10 $\frac{m}{s}$ [4]) and travel long distances each night while continuously solving obstacle avoidance and other navigation tasks reliably. Technical systems cannot match the speed, versatility, and reliability of bats, and typically require much larger amounts of input data (e.g., from laser scanners).

From the current state of research into the biosonar systems of bats, it is not clear what the main factors that enable the superior performance of bats are. However, a look at bat biosonar systems allows for the formulation of hypotheses, one of which, i.e., dynamic time-variant sensing mechanisms, has been investigated in this work.

1.2 Bat biosonar as a model

Bat biosonar encompasses a diverse set of acoustic sensing systems. With approximately 1,200 different species, bats are the second most species-rich group of mammals [5]. About 1,000 bat species utilize some form of biosonar sensing, with an active sonar system, i.e., they analyze echoes that have been triggered by ultrasonic pulses that the animals emit. In addition to active sonar, a significant number of bat species also makes use of passive sonar, i.e., they gain information

through the analysis of acoustic signals that originate from other sources. Using both active and passive biosonar, bats have been able to occupy diverse habitats that range from deserts to rain forests and from coastal marshes to alpine meadows. This ecological versatility has allowed bats to settle almost the entire land surface of the earth; only the polar ice caps and some small isolated oceanic islands are not inhabitated by bats. Within their diverse habitats, bats use their biosonar system to acquire food from a likewise diverse range of sources that include pollen, nectar, fruit, terrestrial and aerial arthropods, fish, small terrestrial vertebrates, birds, other bats, and blood from large vertebrates [6, 7, 8].

The biosonar system of bats is known to be adapted to the different habitats bats live in and the food that they exploit in various ways. For example, bats resort to passive sonar to detect prey that betrays its own presence through sound emission in environments where the presence of many clutter targets would make echo signatures that are unique to the prey unlikely [9]. An example of diversity within the active biosonar systems is the design of the biosonar pulses: Based on their time-frequency structure, bat biosonar pulses can be classified as either frequency modulated (fm) or constant frequency-frequency modulated (cf-fm) [10]. The narrowband (cf) portion of the pulses in the cf-fm bats represents an adaptation to the hunt for flying insects in dense forest environments. It allows these bat species to detect small changes in echo frequency that are caused by the Doppler shifts that are induced through the wingbeat motion of the prey [11]. Since such frequency broadenings are unique to scatterers representing flying prey in the bats' environments, they allow the animals to detect their prey even in dense clusters of clutter targets (e.g., vegetation).

With the diversity in the habitats, diets, and signal designs comes a large morphological diversity in the external structures associated with the bat biosonar system [12, 13]. Bats often diffract the emitted ultrasonic pulses with specialized baffles ("noseleaves") that surround the nostrils in species with nasal emission [14]. In some species with oral emission, conspicuous shape features on or near the lips may play a similar role. Irrespective of emission mode, all bats with biosonar have diverse and often highly unusual shapes of the outer ears (pinnae) that may play a role in the encoding of salient sensory information at the interface between the external world and the internal signal processing that takes place from the transduction stage onwards [13, 12].

Capability and versatility combined with an apparent parsimony (two one-dimensional input signals), make biosonar an attractive model for sensory systems in engineering. However, the key questions such as which mechanisms are responsible for the capability and versatility of the bat biosonar system remain unresolved. Part of the versatility of bat biosonar may be attributable to evolutionary adaptions from the species level upwards. Individual bat species are much more restricted in the food sources that they exploit and in the habitats that they inhabit than bats as a whole. Hence, the biosonar systems of different bat species may have been optimized to perform under certain conditions, but not under others. However, such species-level specializations cannot explain the ability of a large number of bat species to operate in complex, unstructured environments that still pose an unresolved challenge to man-made sensing systems. Hence, it is likely that the biosonar systems of these species have evolved the ability to encode information relevant to the various navigation and foraging tasks they perform in ways that are not yet known to engineering.

1.3 Sensor dynamics in horseshoe bats

Components in the bat biosonar system have adapted to various environments that lead to differences between species evolved over long periods of time. Additionally, recent experimental evidence [15, 16] has shown that critical components in the bat biosonar system have dynamic properties which may not have an equivalent in engineered sensing systems. These critical stages are the baffle shapes that surround the sites of ultrasonic emission (i.e., mouth or nostrils) and reception (i.e, the ear). Because they are located at the interface between the animal and its environment, these structures are in a position to act as gateways that determine what information is encoded in the signals that enter the middle ear. In bat groups with particularly sophisticated biosonar systems [10], such as the horseshoe and Old-World round-leaf nosed bats (families Rhinolophidae [17] and Hipposideridae), the existence of dynamic changes in the baffle shapes (on a subsecond time scale) have been observed.

In horseshoe bats, it has been demonstrated that a major portion of the noseleaf, the anterior leaf

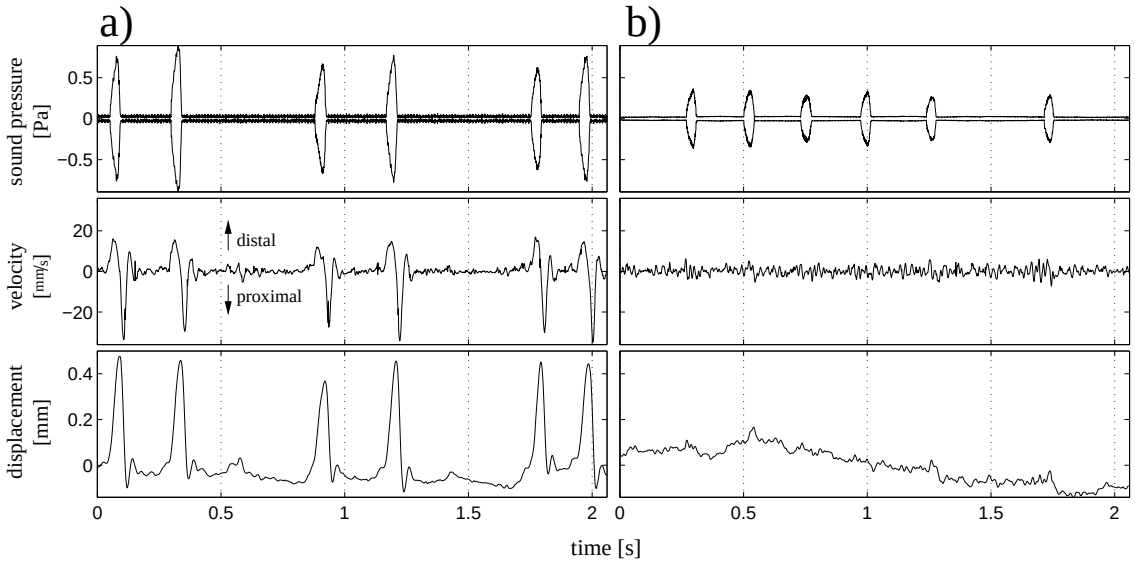

Figure 1.1: Examples of biosonar pulse sequences with synchronized measurements of the velocity of the anterior rim of the noseleaf in the proximal-distal direction: (a) example sequence with non-random motions of the anterior leaf. (b) example sequence without non-random motions. For each example, the top graph shows the envelope of the sound pressure amplitude, the center graph the velocity, and the bottom graph the displacement amplitude of the anterior rim of the noseleaf in the proximal-distal direction. Positive velocities and displacements correspond to motions in the distal direction (i.e., away from the head). Reproduced from [16]. See page 2 of copyright permissions document.

that forms a semicircular cone-shaped baffle around the lower portion of the nostrils, can undergo dynamic shape changes [16]. It was found that the walls of the anterior leaves can carry out an inward twitching motion that was tightly correlated with the emission of the pulses. That is, the maximum surface velocities and the maximum displacement values were always reached within the duration of the emitted pulse (s. Figure 1.1). The amplitude of the measured deformations – as large as 0.75 mm on each side of the baffle – can be considered as significant compared to the wavelengths employed by the bats (about 4 mm for the narrowband portion of the pulses). It was further observed that the bats had active control over the twitching motion of the anterior leaf and were able to turn it on or off [16]. This observation has been interpreted as evidence against the hypothesis that the noseleaf motions are byproduct of the pulse emission process [16]. Instead, the accurate temporal alignment of the twitching motion with the pulses combined with

the evidence for active control can be taken as evidence for a functional role of these deformations. However, what specific function these effects may have remains unknown. A hypothesis proposed by Kuc [18] according to which noseleaf vibrations at the ultrasonic carrier frequency could act as a transduction mechanism was not supported by the experimental vibration data from the anterior leaves of horseshoe bats [16].

Similar to the noseleaves, the pinnae (outer ears) of horseshoe bats have also been found to undergo dynamic shape changes [15]. The pinnae are located at an important interface between the external environment and the sensory system and hence are in a position to control the primary encoding of sensory information. They diffract the incoming echoes in a direction and frequency dependent manner and thus define a joint direction-frequency selectivity filter that determines what information is encoded for downstream processing and how. Through executing this encoding process, the pinnae perform an important signal processing operation in the physical domain that may not be readily accomplished in the neural domain. This potential importance of the pinnae may explain the large morphological diversity in the pinnae of bats, part of which could represent adaptations of the sensory encoding process to different biosonar tasks and constraints faced by different ecological niches that the bats occupy.

At the level of individual behavioral adaptations, dynamic changes to the pinna shape may likewise have a functional importance. This notion is supported by early anatomical findings in horseshoe bats [19] that show that these animals have an unusually large number of ear muscles (approximately 20) with elaborate muscular actuation mechanisms. The pinna muscles can be categorized into two groups. In one group, the insertion points extend from the skull to the pinna. Both end points on the second group of muscles are located on the pinna cartilage (s. Figure 1.2). Hence, these muscles can not only effect rigid rotations (i.e., forward and backward motion) but also non-rigid deformations (i.e., changes in the geometry of the pinna).

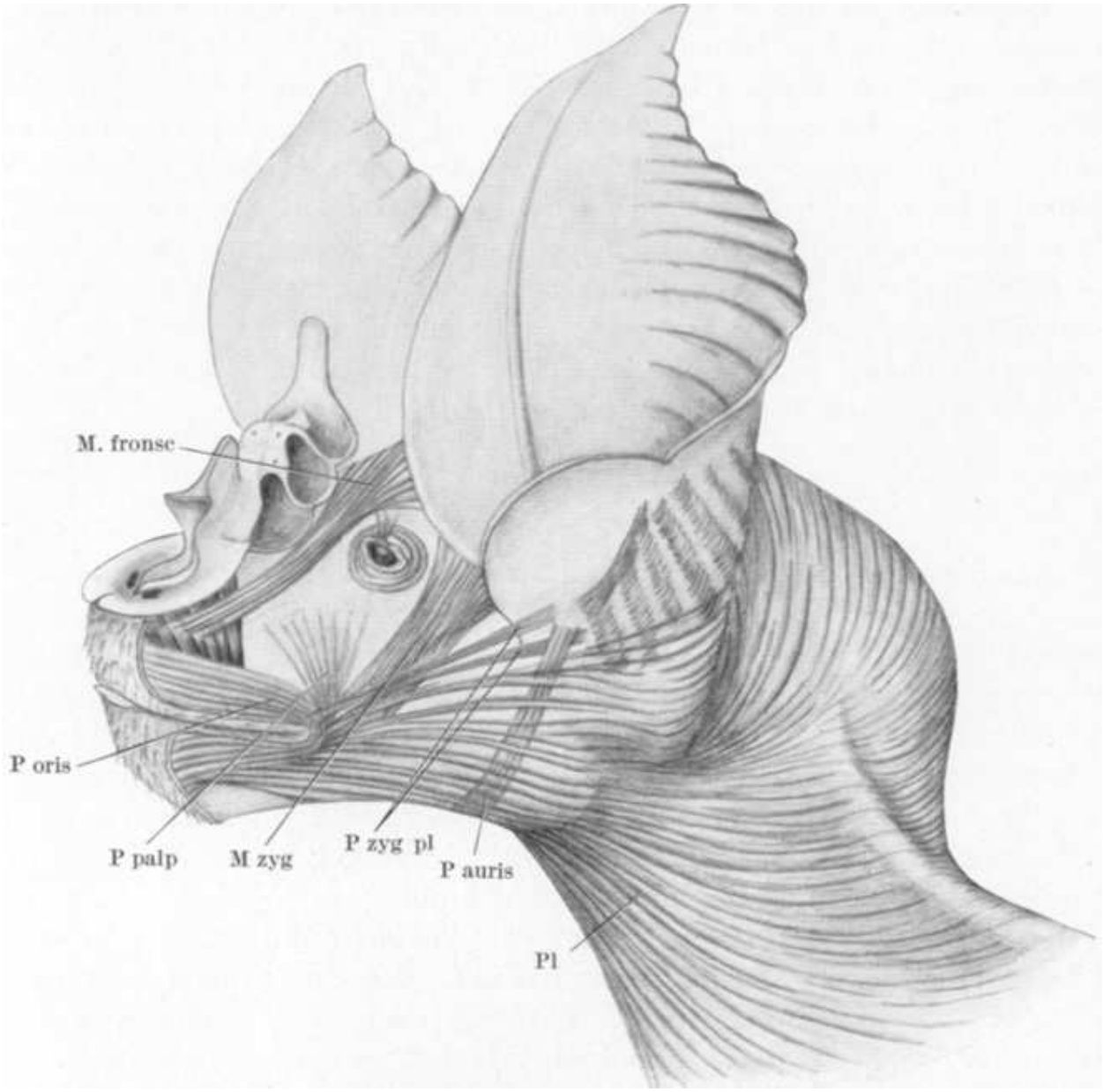

Figure 1.2: Some of the muscles in the outer ear of the greater horseshoe bat (*Rhinolophus ferrumequinum*). From [19], reproduced with permission. See page 3-8 of copyright permissions document.

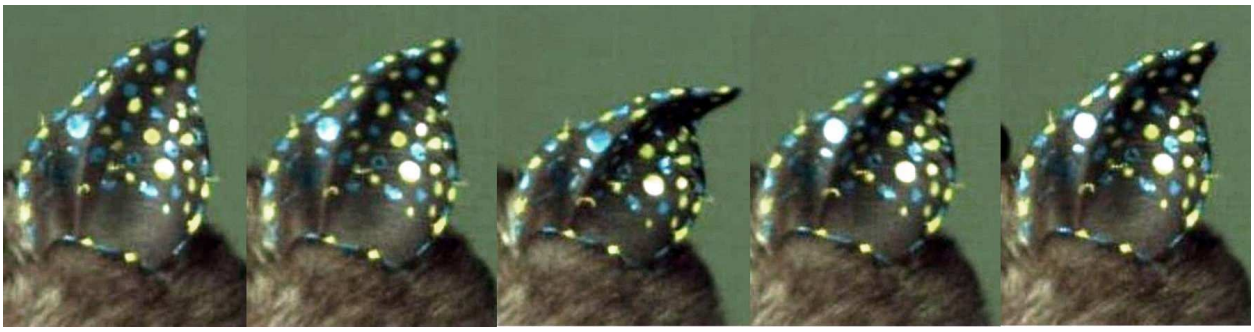

Figure 1.3: Frames from a high-speed video-recording of the ear deformation of the horseshoe bat.

Results from behavioral experiments [20] also point to the importance of pinna motions in horseshoe bats: In these experiments, the bats' target localization performance was tested by the ability of the animals to navigate arrays of horizontal and vertical wires placed into their flight path. The role of pinna motions was then tested by cutting the motor nerves and muscles in the pinna. Immobilizing the pinnae in this way was found to degrade the localization in vertical direction significantly but not in the horizontal direction [20]. This finding could in principle be explained through the rigid rotation of the pinnae alone, which would allow the animals to use the narrow-band portions of their biosonar pulse for direction finding through observing the amplitude of the echo returns during a scan [21]. This would provide the horsehoe bats with an alternative mechanism to fm-bats which can use spectral signatures imprinted onto their broadband signals for direction finding. However, though these findings provide an overall measure of performance, they do not contain information regarding the relative importance of different aspects of the pinna motions that may have been affected by the surgery.

The current work focuses on the non-rigid component of the pinna dynamics in horseshoe bats. High-speed recordings (s. Figure 1.3) of horseshoe bat pinna clearly show non-rigid deformations of the pinna geometry that can be completed within cycle times below 200 ms [15]. These deformations arise due to the intricate muscular actuations [19] in the bat pinna which can occur both in flight and when the bat is stationary.

Three-dimensional digital models [22, 23] of this time-varying behavior have been obtained from stereo high-speed video recordings and have been used to characterize both the geometry and the

acoustic effects of these deformations in detail: These recordings show that during a non-rigid deformation, the tip of the pinna moves down and to the side while the anterior portion of the pinna wall moves more than the posterior. The maximum total deformation has been estimated at around 20 % (i.e., $\sim 4\,\mathrm{mm}$) of the total height of the pinna ($\sim 2\,\mathrm{cm}$). The acoustic effects of this deformation has been predicted numerically and were found to be substantial and of a qualitative nature [24, 15]. However, these numerical predictions were limited to frequency-domain characterizations in which the signal characteristics did not change within the length of the analysis window.

1.4 Objective and Approach

The work presented in this thesis has been aimed at gaining greater depth in understanding the non-rigid deformations of the horseshoe bat pinna as a dynamic physical and sensory process. To this end, two fundamental questions were asked:

1. What is the relationship between the geometry of the pinna and its acoustic properties? - Of particular interest in this context are the conspicuous local features of the horseshoe bat pinnae and the potential role that they could play in the context of the dynamic changes in the overall pinna shape.

2. Is there an effect of baffle deformations like the ones seen in pinna shape on the function of the device as a gateway for sensory information? In particular, can it be determined experimentally whether pinna-like baffle deformations result in an enhanced capacity for the encoding of sensory information?

Pinna deformations have several properties that turn an in-depth analysis *in-vivo* into a challenge: the static shapes and their deformation patterns are fairly complicated and the deformations happen very quickly and appear to be part of rather flexible behavioral patterns that could be difficult to

repeat in an identical fashion, making it hard to accomplish through behavioral experiments with bats.

At present, experimental paradigms exists in which a miniature measuring microphone is mounted in the animals' ear canal. Sounds emitted from a speaker positioned in different directions from the bat are then recorded by this microphone to characterize the outer ear's influence on the transfer function between the speaker and microphone. This experimental approach has been used successfully to measure stationary head-related transfer functions in bats. However, it is not likely to permit the measurement of non-stationary responses from deforming baffle shapes. To achieve this, the bats would have to repeat the same pinna movements hundreds if not thousands of times with change in sound direction, while keeping the overall position of the head and pinna constant. For a fine angular and temporal sampling of the acoustic effects, on the order of 10^4 deformation cycles could be required. This would be impossible to achieve with an animal subject, no matter whether the animal is awake or anesthetized. In either case, data collection could not be accomplished in a single session, and reproducibility between sessions would become a problem. In an awake animal, movements of the head or overall rotations of the ear would be additional confounding factors.

It has yet to be established whether ear deformation could be reliably and repeatably be triggered in an anesthetized animal. Even if this was the case, keeping the same animal alive through a sequence of many long anesthesias would be a challenge. Furthermore, it would be difficult to synchronize the emission of the test signals to specific phases of the ear deformation cycle. A large variability in the initiation of the ear deformation is to be expected in awake animals and for anesthetized animals it would have to be seen how accurately and reproducibly the ear deformations could be triggered, if at all.

Because of all these drawbacks, the work presented in this thesis has focused on using a biomimetic modeling approach to this problem. For this purpose, a simplified deforming prototype was created to allow for an easier analysis of static and dynamic shape features as well as for a complete acoustic characterization of the deforming prototype's time-variant linear behavior as a function of

direction. This approach not only removes the difficulties associated with in-vivo experiments, it also offers a number of critical advantages:

1. A synthetic system gives more freedom to change every aspect of the baffle (e.g., global and local shape features, as well as their dynamics).

2. An automated setup allows collection of large amounts of data under repeatable conditions for all these different modifications.

3. A simplified prototype offers a greater chance to understand the physical processes that are responsible for the observed effects.

4. An artificial model provides an additional opportunity to test static and dynamic configurations that are not realized in bats, but could be insightful and lead to interesting technical solutions.

1.5 Chapter outline

The remaining chapters of the document have been organized as follows:

Chapter 2 describes the simplified biomimetic ear prototype, local shape features selected from observing the greater horseshoe bat and fabrication methods that lead to a parsimonious and simple model.

Chapter 3 describes the experimental setup for the prototype, data characterization and finally signal processing of the data.

Chapter 4 presents the results obtained from the experimental simulations and discusses the interplay of static and dynamic features of the prototype.

Chapter 5 presents a novel method of analyzing the data through an information theoretic approach for determining the sensor coding capacity of the deforming ear prototype.

Chapter 6 summarizes the work performed so far and presents suggestions for future work.

Chapter 2

Biomimetic Prototype

(This chapter was published in part in Bioinspiration and Biomimetics, doi: 10.1088/1748-3182/8/2/026008. Reproduced with permission [25]. See page 9 of the copyright permissions document.)

The deformation patterns observed in the horseshoe bat pinna, as described in the previous chapter, are highly complicated. The pinna deformations between upright and bent positions occur at very high speeds, i.e., on time scales of milliseconds. To mimic such deformations and understand their possible functional implications, a biomimetic prototype was created which incorporated a controlled deformation in a simplified manner. Besides simplification, the advantages of using a biomimetic prototype is the greater control over local shape features as well as the dynamic behavior.

2.1 Simplified prototype: basic shape

The biomimetic prototype designed here was intended to represent a simplified shape of the pinna while preserving the important functional features. To achieve this goal, the general shape of the bat pinna has been approximated as an obliquely truncated cone augmented with local shape features. This obliquely truncated cone shape had already been suggested as a simplified model

for the general mammalian pinna [26, 27].

For bats in particular, this intuition has since been supported by virtue of a quantitative analysis conducted with a data set consisting of 100 different bat pinna shapes representing at least 50 bat species [12]. This analysis was based on accurate and detailed digital three-dimensional models of bat pinna shapes that had been obtained from biological samples using micro-computer tomography. These shape models were transformed into vector representations by expressing the location of discrete pinna surface elements in a cylindrical coordinate system. Each pinna shape was represented by a feature vector that contained the radius values for the pinna surface elements as a function of direction and height. In this vector space, the average pinna shape could be determined through a vector sum and was found to resemble an obliquely truncated horn.

The first eigenear, i.e., the eigenvector associated with the largest eigenvalue, obtained from the principal component analysis (PCA) in the vector space was also found to approximate the shape of an obliquely truncated horn. To describe the variability in the natural pinna shapes, a weighted version of the eigenears is added (or subtracted from) to the average pinna. Since the geometry of the average pinna and the first eigenear were both found to resemble obliquely truncated cones, most of the variability in bat pinna shapes can be understood as cones of varying opening angles.

However, the averaging operation that gave rise to the obliquely truncated cone approximation erases information on local shape features. Such features were also not readily accessible in the PCA, since components of higher spatial frequencies were required from the eigenears. In principal component analysis, the components are also sorted based on their spatial frequency content, i.e., the components associated with the largest eigenvalues also tend to represent low spatial frequencies. Hence, pinna shape features from higher spatial frequency bands were distributed across eigenears (eigenvectors) associated with lower eigenvalues that were difficult to estimate and interpret reliably. Hence, in the present work, the obliquely truncated cone was chosen as a model for a simplified overall pinna shape to which local shape features were introduced that were inspired specifically by the pinnae of horseshoe bats.

2.2 Local shape features

The echolocation frequencies for the bats can range from audible range to high frequencies over 100 kHz, as seen in some horseshoe bats [28, 29]. Due to such high frequencies, the wavelengths of the ultrasonic pulse echos received at the bat pinna can be as small as 3.4 mm or even shorter. At such small wavelengths even comparatively small, local shape features could be functionally important. In accordance with this prediction, previous work has produced evidence for the importance of various local pinna features in other bat species. One such feature is the tragus, which is a protrusion of the anterior pinna rim [30, 31], presumably through the generation of sidelobes in the beampattern [31, 32, 33]. The tragus in many bat species is much more prominent than it is in other mammals such as humans. Deflecting the tragus in the big brown bats (*Eptesicus fuscus*) has been shown to have a strong effect on the accuracy of angle perception in vertical direction [30]. Similar results were obtained from numerical beampattern estimates that were used to study the effect of a small ridge on the interior wall of the pinna of the long-eared bat (*Plecotus auritus*) [34]. An acoustic function has also been hypothesized for the washboard ripple that can be found on the inner wall of the pinnae in a significant number of bat species, including horseshoe bats. In the big brown bat, a hypothesis has been formulated [35] that posits that the washboard ripple and the tragus form an acoustic lens to focus high frequency energy (up to about 150 kHz) into the ear canal. However, these predictions are not in a good agreement with the upper limit of the biosonar pulses recorded for the big brown bat.

The importance of local features has been evident from the emission beampatterns as well. The presence or absence of the resonant cavities [36, 37] and the sella [38, 37] in the noseleaf structures have shown varying effects in the beampatterns. However, noseleaves and pinna local features may serve for different functional importance. Noseleaves lead to emission beampatterns due to the emitted pulses and pinna diffract the incoming echos for reception beampatterns. The attenuation of incoming echos is much higher than compared to the emitted pulses.

Thus, considering the circumstantial evidence from noseleaf local features and the various local feature effects from the pinna shapes, in this work an obliquely truncated cone geometry aug-

mented with biomimetic local features was developed. This device could thus be a way to provide additional experimental insight into the possible acoustic effects of local shape features and the underlying physical mechanisms.

2.3 Prototype fabrication

In order to simplify manufacturing, actuation, and acoustic characterization, the biomimetic prototype was created at a size larger than that of the pinna of the greater horseshoe bat (*Rhinolophus ferrumequinum*) which served as a model species for the present work. Whereas the pinnae of this species are about 2 cm in length, the biomimetic prototypes were scaled up two and half times to a total length of 5 cm. The material thickness was not scaled since it is not expected to impact acoustic diffraction and hence beamforming. The biosonar pulses of these animals typically cover in the frequency range of 60 kHz to 80 kHz with the cf-component being located at the upper end of this range. By scaling the analyzed frequency range down to 24 kHz to 32 kHz for the prototype, the ratio between wavelength and baffle size was preserved.

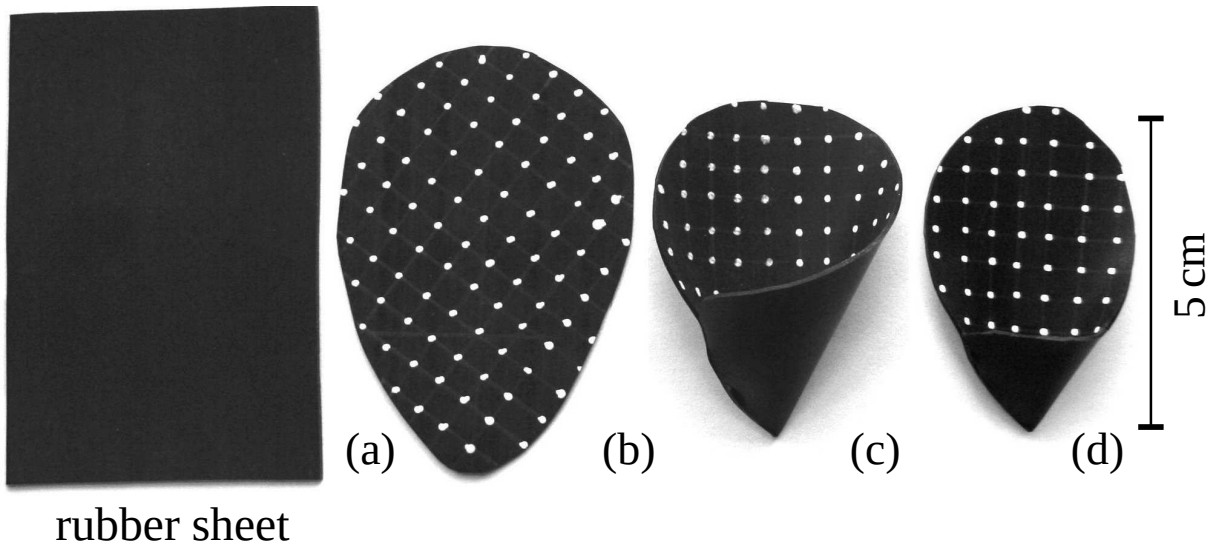

Figure 2.1: Fabrication of the basic prototype shape: (a) isobutyl rubber sheet, (b) leaf-shaped cutout, (c) cutout folded at one end, (d) trimmed to the final truncated cone shape.

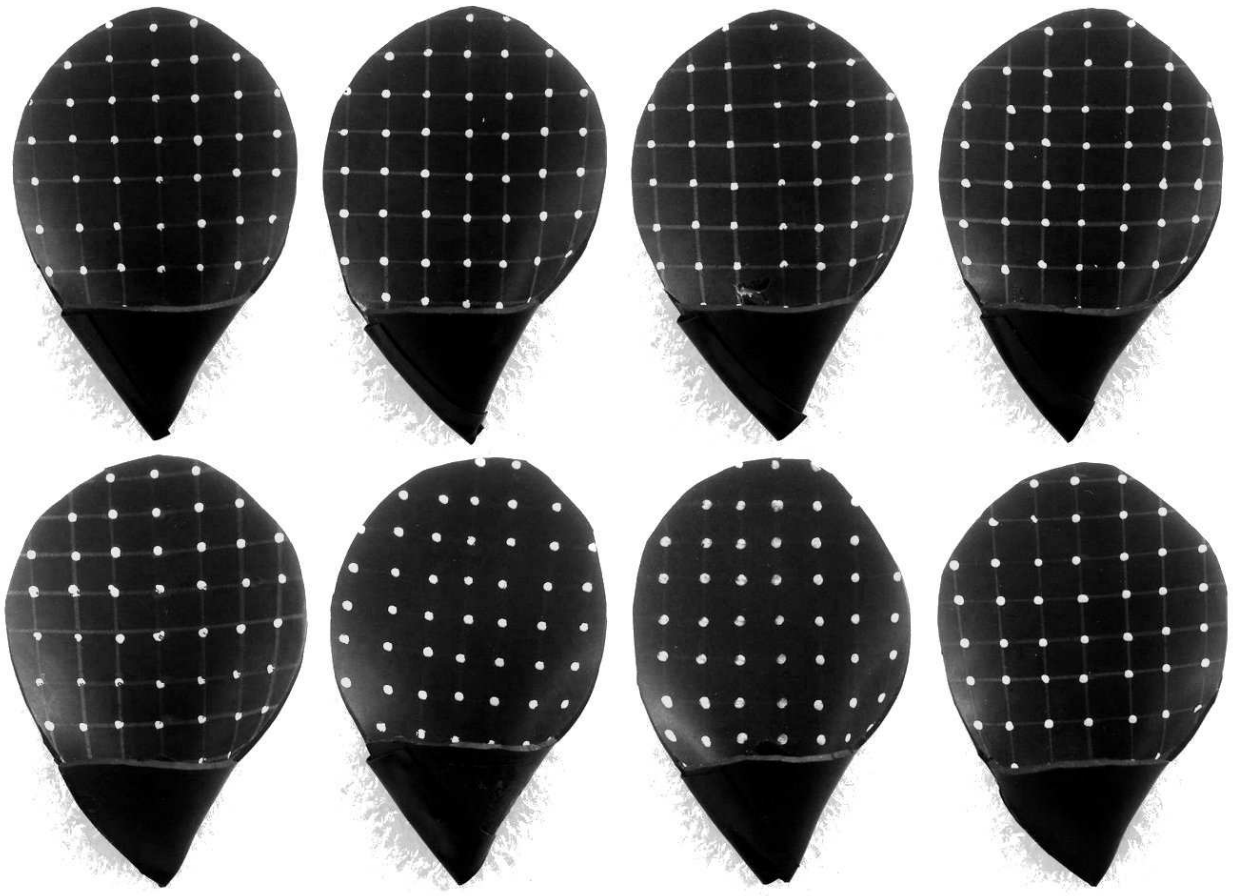

Figure 2.2: Eight plain cone prototypes manufactured for testing the reproducibility of the beam-patterns and repeatability of the fabrication method.

The ear prototypes were manufactured from a millimeter-thick, planar isobutyl rubber sheet in order to create a flexible prototype capable of non-rigid deformation. The rubber sheet was cut into a leaf shape with a length of 10 cm. To create a shape of an obliquely truncated cone, one end of the sheet was folded towards a curved edge at a distance of 3 cm. The folded sheet was given a final trim to obtain the shape of a truncated cone (s. Figure 2.1). Eight such plain cone prototypes were manufactured before augmenting them with local features (s. Figure 2.2).

There were some clearly visible local features in the pinna of the horseshoe bat. Three such features were chosen based on their potential acoustical importance and mechanical functionality. These features were: (i) a vertical ridge, (ii) an incision on the pinna rim, and (iii) the antitragus

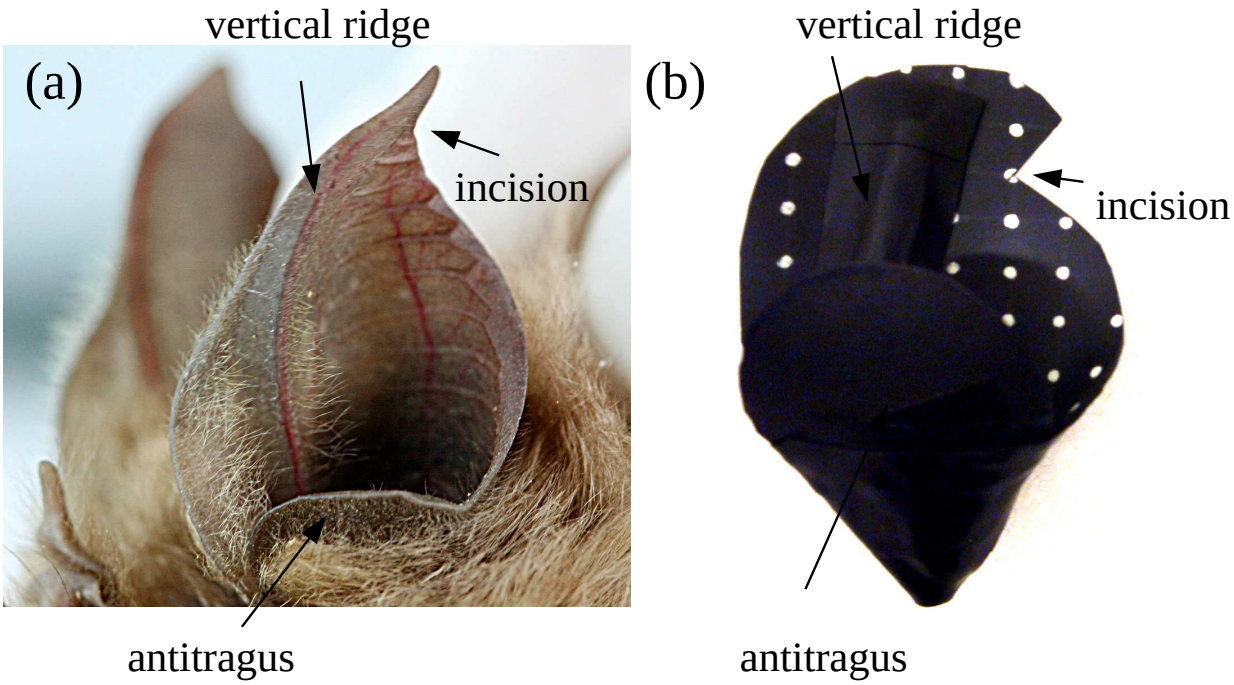

Figure 2.3: Comparison of a horseshoe bat pinna with the simplified prototype: (a) local shape features extracted from the greater horseshoe bat, (b) plain cone augmented with the local features.

(s. Figure 2.3). The vertical ridge was modeled by attaching additional material to the anterior wall of the pinna, the incision was made by cutting the rubber sheet at its rim, and the antitragus was represented by a rubber flap at the proximal end of the cone. All three features broke the original left-right symmetry of the plain cone. The size of the shape features to the over all ear was approximately the same as the horsehoe bat pinna.

Since the local shape features were each located in a different region of the prototype, they could be placed and removed independently of each other. To study possible interactions between their acoustic effects, prototypes that represented a complete set of all combinations of these features were created (s. Figure 2.4). This set contained a total of eight prototypes: the plain cone without any local features, three prototypes augmented with a single feature each, three prototypes augmented with two features, and one prototype augmented with all three features (s. Table 2.1).

prototype #	ridge	incision	antitragus
1			
2	+		
3		+	
4			+
5	+	+	
6		+	+
7	+		+
8	+	+	+

Table 2.1: Overview of the analyzed set of biomimetic baffle prototypes.

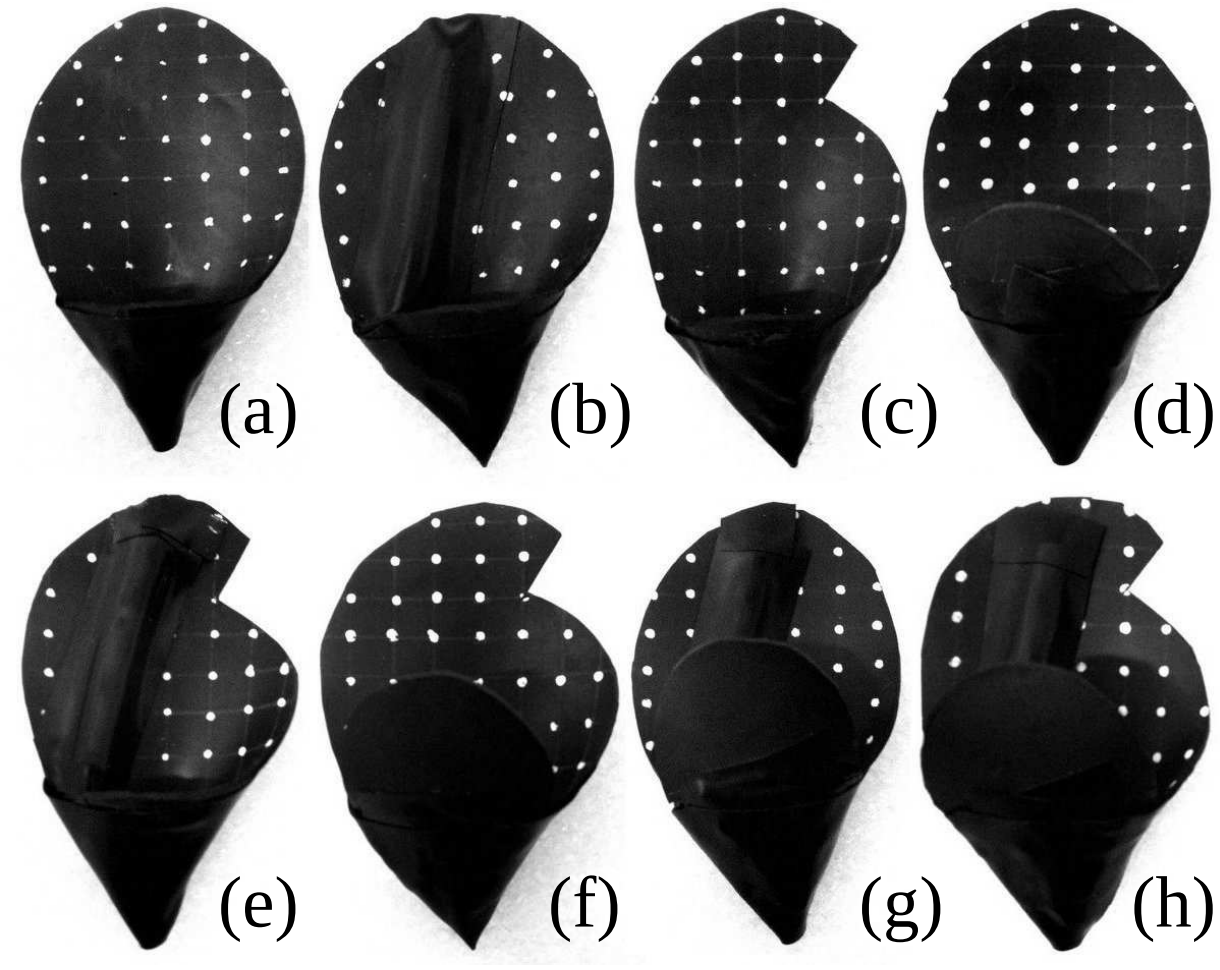

Figure 2.4: Set of prototypes augmented with biomimetic shape feature combinations: (a) no features, (b) ridge, (c) incision, (d) antitragus, (e) ridge and incision, (f) incision and antitragus, (g) ridge and antitragus, (h) ridge, incision, and antitragus.

Chapter 3

Experimental Characterization

(This chapter was published in part in Bioinspiration and Biomimetics, doi: 10.1088/1748-3182/8/2/026008. Reproduced with permission [25]. See page 9 of the copyright permissions document.)

3.1 Actuation mechanism for the dynamic deformation of the prototype

The biomimetic prototype was fixed onto a hemispherical styrofoam ball. The arrangement was chosen to mimic the head of the bat and shield sound reflections from system components that were mounted immediately behind the prototype (s. Figure 3.1). A digital servo motor (Hitec HS-5485HB) was installed behind the styrofoam ball (s. Figure 3.1b) to produce the deformations of the prototype using a single-point actuation mechanism. For this purpose, the servomotor and the prototype were coupled through a lever [39]. The lever pushed the prototype from behind in the same region where also the vertical ridge was mounted on the opposite side of the prototype wall, if present. This particular location was chosen to mimic the deformation of bending and lateral rotation that has been described from the high-speed video recordings of the horseshoe bat pinnae (s. Figure 1.3).

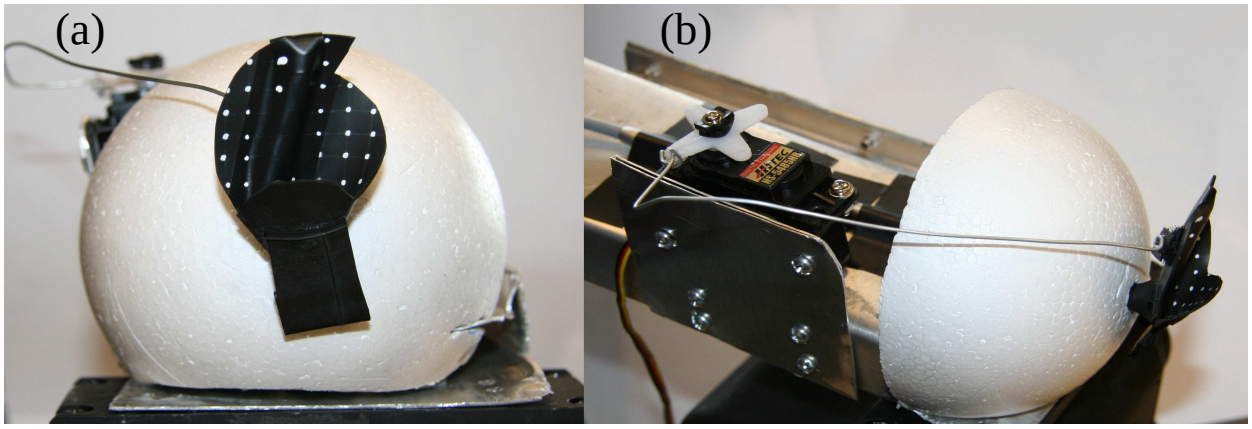

Figure 3.1: Single point actuation mechanism of the biomimetic prototype: (a) front view, (b) side view.

Figure 3.2: Seven shape changes from upright to bent configuration in the ear prototype.

Deformation from upright to bent positions was carried out in a small number of discrete steps, typically seven, each of which were characterized acoustically (s. Figure 3.2). The upright to bent positions in the ear prototype resulted in about 20% deformation compared to the total height of the prototype of 5 cm. Since bending deforms the ear, the relative position and orientation of the features were also changed. The servomotor was controlled through an input from the data acquisition system, described in the next section.

3.2 Experimental setup

In order to characterize the acoustic properties of the prototype, the prototype and its actuation mechanism were mounted on a pan-tilt unit: FLIR Motion Control Systems (D48 E-series unit, s. Figure 3.3). The pan-tilt unit was then placed in the far-field region at a distance of one meter from the ultrasonic loudspeaker (Ultrasound Advice S56 with Ultrasound Advice S55 amplifier) that served as a source for the acoustic input signals (s. Figure 3.4). Sound incidence from different directions was achieved by rotating the prototype while the ultrasonic loudspeaker stayed in place. Using this paradigm, acoustic characterizations of the prototype were obtained for directions that were spaced three degrees apart over a range of 180° (-90° to +90°) in azimuth and 120° (-30° to +90°) in elevation.

Figure 3.3: Actuation setup mounted on the Pantilt unit.

As an acoustic input for the acoustic characterization, linear frequency modulated chirp signals with a duration of 2 ms covering the frequency range of 10 kHz to 100 kHz were emitted from the ultrasonic loudspeaker.

The response of the prototype was recorded through a microphone: Brüel and Kjær 4138 1/8” pressure-field microphone that was coupled with the prototype through a polyvinyl chloride (PVC) tube of matching diameter (4 mm) and 6.5 cm in length in the style of an “ear canal” with an opening located on the proximal wall of the prototype. The microphone was mounted behind the styrofoam hemisphere, so that the connecting tube was straight.

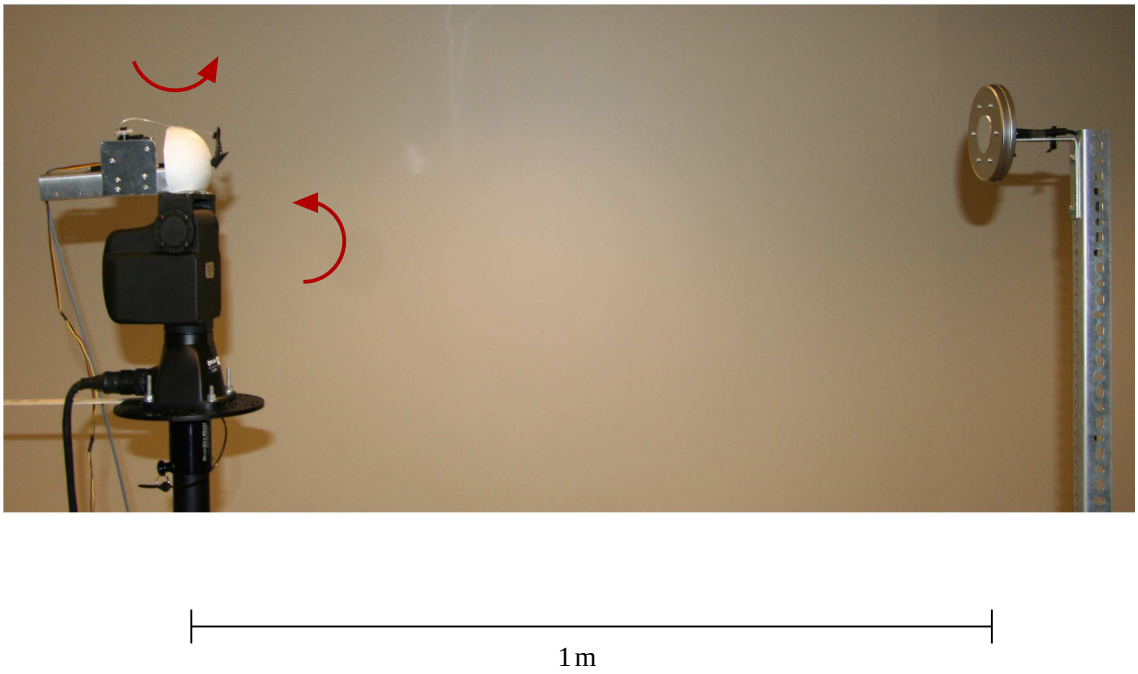

Figure 3.4: Experimental Setup: The ear prototype is placed at a far field region with respect to the loudspeaker.

The microphone signals were conditioned with a preamplifier: Brüel and Kjær Type 2690 before they were digitized. Digital data was acquired using a PXI data acquisition system: National Instruments PXI-1033 chassis with PXI -7852 R Virtex-5 LX50 R series Multifunction RIO module operating at a sampling rate of 1 MHz and 16-bit resolution. The data acquisition system was also used to create the ultrasonic pulses emitted from the loudspeaker with a conversion rate of 1 MHz with 16 bits of resolution as well as to control the actuation of the prototype and the pan-tilt unit [40].

The overall setup (s. Figure 3.5) was positioned at a minimum distance of at least one meter (typically more) from any surrounding surfaces such as walls, floor or ceilings so that reflections from these objects could be excluded by a suitable recording time window.

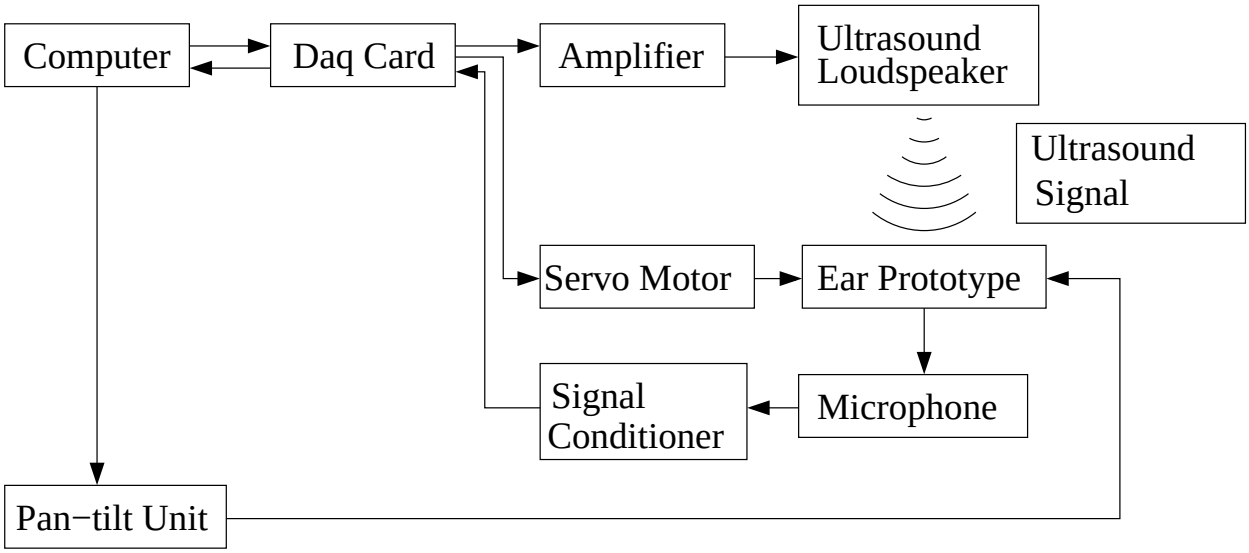

Figure 3.5: Block diagram of the automated characterization setup.

3.3 Time-variant signal processing

The time domain signals at 2501 positions in the direction space were recorded in response to the input pulses. These signals were transformed into a frequency domain using a fast Fourier transform with a length of 4096 points and a rectangular windowing function to obtain a spectrum for each point in the direction space. The values of the spectral coefficient across the direction space were then used to describe the beampattern of the device for a given deformation stage and at a certain frequency (s. Figure 3.6).

Initially, the eight plain cone shapes were subjected to the experimental simulations at static positions. After that, the prototypes augmented with local shape features were simulated experimentally.

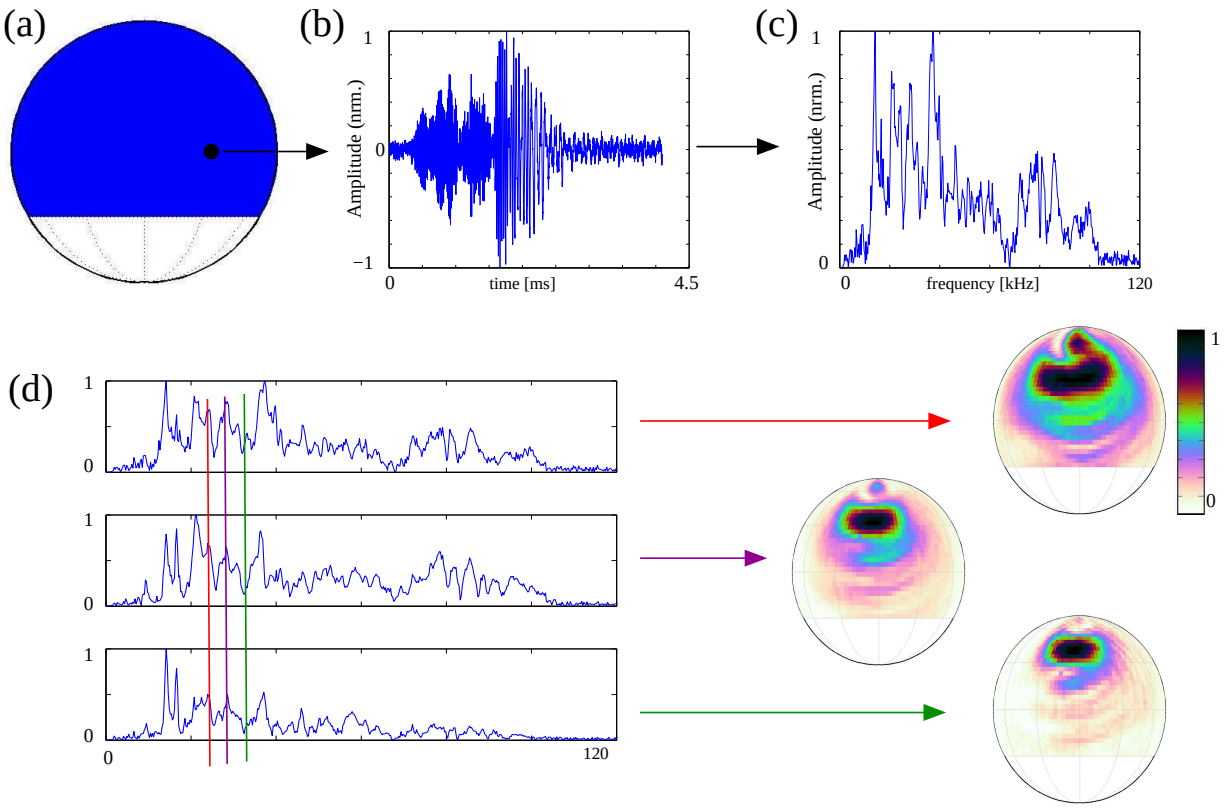

Figure 3.6: Time-variant signal processing: (a) spatial direction of the recorded signals, (b) recorded signal at one particular position in the direction space, (c) amplitude spectrum after fast-Fourier transforming the signal and (d) beampatterns for frequencies obtained by combining the spectra.

Chapter 4

Local Shape Features

(This chapter was published in part in Bioinspiration and Biomimetics, doi: 10.1088/1748-3182/8/2/026008. Reproduced with permission [25]. See page 9 of the copyright permissions document.)

4.1 Reproducibility

Since the prototypes developed were not machine manufactured, it was important to assess the reproducibility of their acoustic properties. As explained in the second chapter, one of the manufactured shapes, the plain cone which is an abstraction of the average bat pinna without any local features, was replicated eight times (s. Figure 2.2) as a mass production.

The acoustic sensitivity for each of the static-plain cones prototypes was experimentally characterized. The reception beampatterns measured for the eight plain cone shapes were found to be in good qualitative agreement. For each of the realizations, the beampattern was dominated by a single mainlobe that decreased in width as the analyzed frequency was increased (s. Figure 4.1). The beampatterns of the different replicates were, however, not identical in every detail.

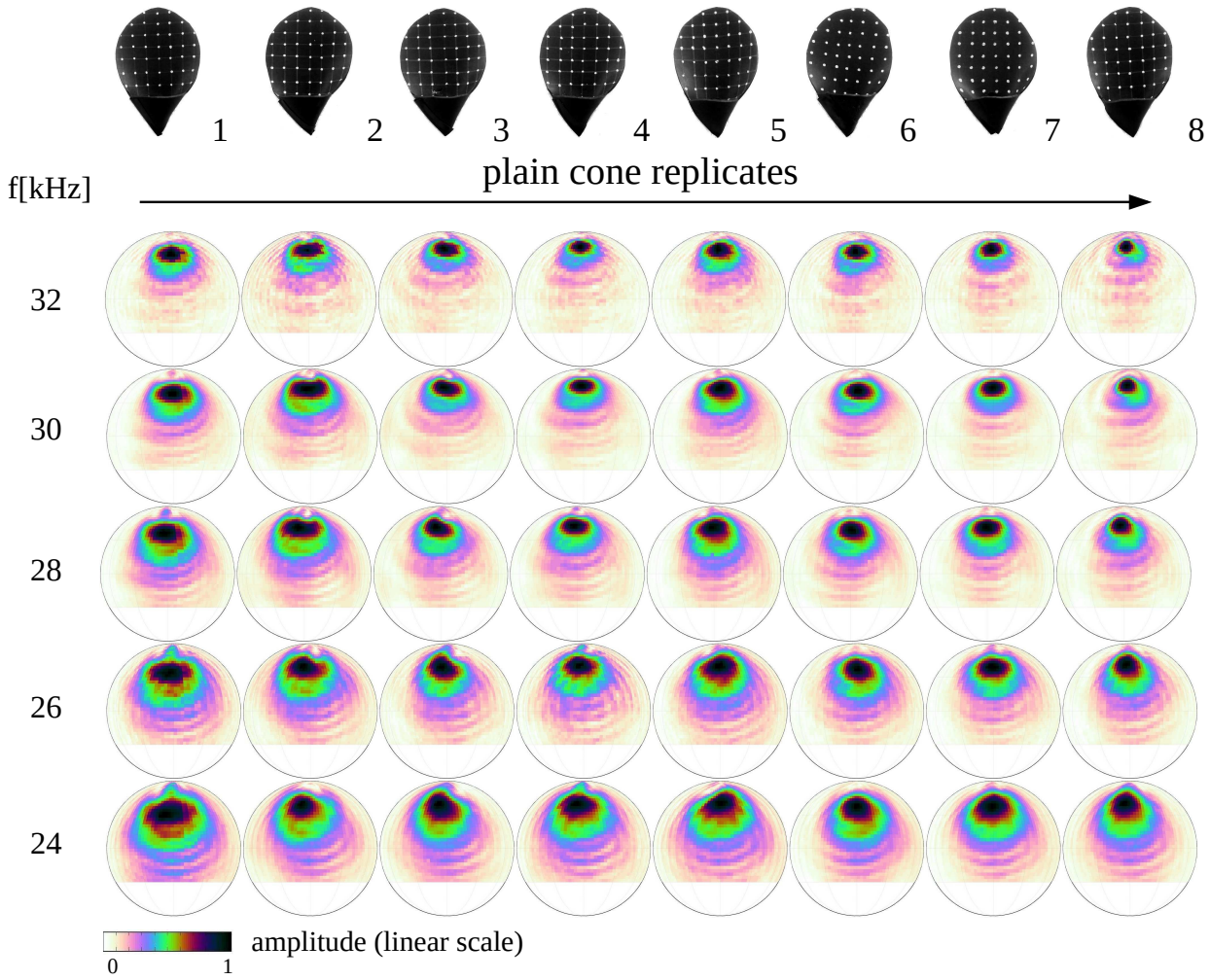

Figure 4.1: Reproducibility of the results: Beampatterns obtained from the different realizations of the plain cone shape. Rows from bottom to top are patterns at frequencies of 24 kHz (corresponds to 60 kHz in bats) to 32 kHz (corresponds to 80 kHz in bats) at an interval of 2 kHz. The columns represent the plain cone prototypes.

4.2 Plain cone behavior

Shape deformations did not cause any major effects on the plain cone beampatterns. At the upright stage, beampatterns showed a prominent single mainlobe with few poorly distinguished sidelobes.

The mainlobes narrowed significantly with increasing frequency, as seen in the static plain cone results.

When the plain cone shape was subject to deformation, beam gain values were changed but over all nature of the beampatterns remained the same (s. Figure 4.2). The changes were comparable to the variations between the beampatterns seen across the different realizations of the plane cone in the upright position (s. Figure 4.1). The general, qualitative nature of the beampattern, i.e., a single prominent mainlobe with few poorly distinguished sidelobes and a monotonic inverse relationship between frequency and beamwidth, remained largely unaffected by the deformation (s. Figure 4.2).

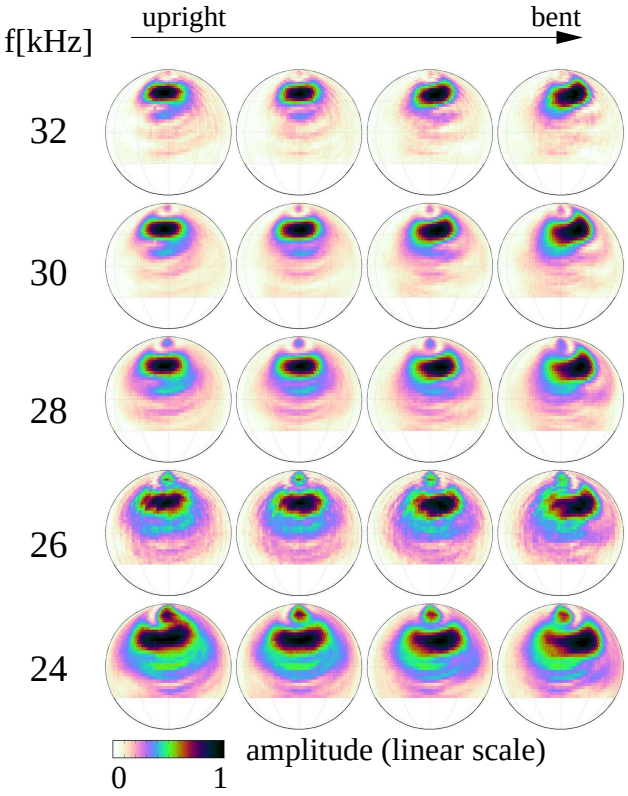

Figure 4.2: Beampatterns at various bending stages for plain cone shape. Rows represent the frequencies from 24 kHz for prototype (corresponds to 60 kHz in bats) to 32 kHz for prototype (corresponds to 80 kHz in bats) at an interval of 2 kHz. Columns represent bending stages from upright to bent.

4.3 Interplay between shape features

Various trends were observed after analyzing the beampattern behavior after augmenting the plain cones with local features. When each of the three local shape features was added to the plain cone shape in isolation, the changes that occurred in the corresponding beampatterns were generally small. The magnitude of these effects hardly exceeded the range of the observed individual variations between the different realizations of the plain cone or the bending stages of the plain cone. This was the case for the ridge (s. Figure 4.3, second row from the top). In the case of the antitragus being added to the cone in isolation, the beampattern effects were much more systematic and pronounced, resulting in a shoulder that extended downwards in elevation from the mainlobe (s. Figure 4.3, third row from the top). The incision made to the plain cone resulted in reduction to the size of the mainlobe in the beampatterns (s. Figure 4.4, third row from the top).

However, when the ridge and antitragus features were added to the plain cone as a combination, the resulting changes to the beampattern were much more pronounced than the changes associated with the addition of each individual features: In this case, a prominent sidelobe occurred in the beampattern which was most pronounced in the bent deformation stages, where its shape also depended strongly on frequency: for low frequencies, the sidelobe's sensitivity was spread out over a wider range of directions, whereas it was more concentrated for high frequencies (s. Figure 4.3, bottom row).

Similarly, the beampatterns of the cone shape that had been augmented with a combination of a ridge and an incision showed a strong dependence on bending stage with a sidelobe that grew more pronounced as the prototype's tip was bent down (s. Figure 4.4, bottom row). For this feature combination (ridge and incision), the beampattern changes in the upright position were small and gradual, as was the case for the individual changes. In the bent position, however, changes are large and quantitative in the sense that a large sidelobe appears that was not present in the beampatterns of either the ridge or the incision as individual features (s. Figure 4.4, bottom row).

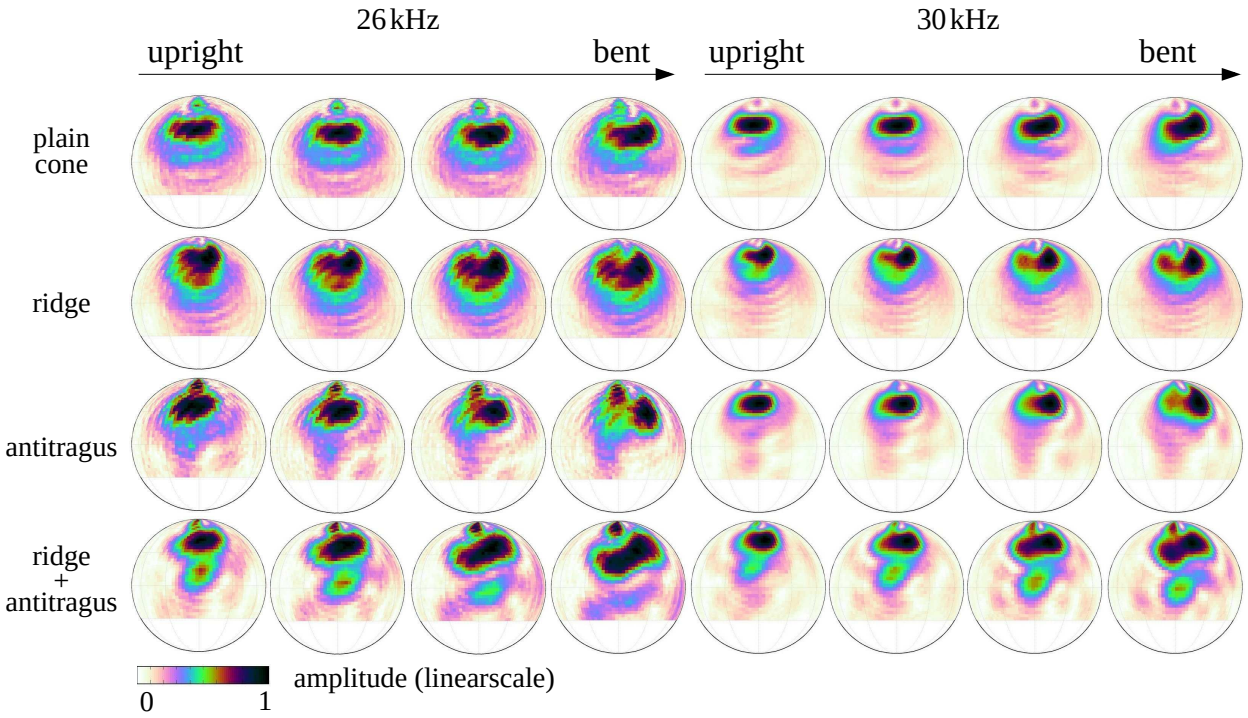

Figure 4.3: Beampatterns at various bending stages for cone shapes augmented with individual shape features or feature combinations: Two frequencies, low (26 kHz for prototype corresponds to 65 kHz in bats) and high (30 kHz for prototype corresponds to 75 kHz in bats), are shown for each feature combination and bending stage.

4.4 Quantitative analysis of the beampatterns

Using the beampattern data, a further quantitative analysis was performed by representing each sidelobe in the beampattern by its maximum amplitude value. All the sidelobe maximum amplitude values of a beampattern were summed into a single measure representing the prominence of the sidelobes, the “amplitude-weighted sidelobe numbers” (s. Figure 4.5). Higher value of the amplitude-weighted sidelobe number signifies higher strength of the sidelobes in the beampattern. Amplitude-weighted sidelobe numbers were calculated for all the beampatterns of all feature combinations, bending stages, and frequencies (s. Figure 4.6). This data also showed indications of interactions between the combinations of the local shape features and bending stage. The number of sidelobes and their strength was with a few exceptions greater for shapes with multiple features than for those with a single feature; this difference was increased with increased bending of the

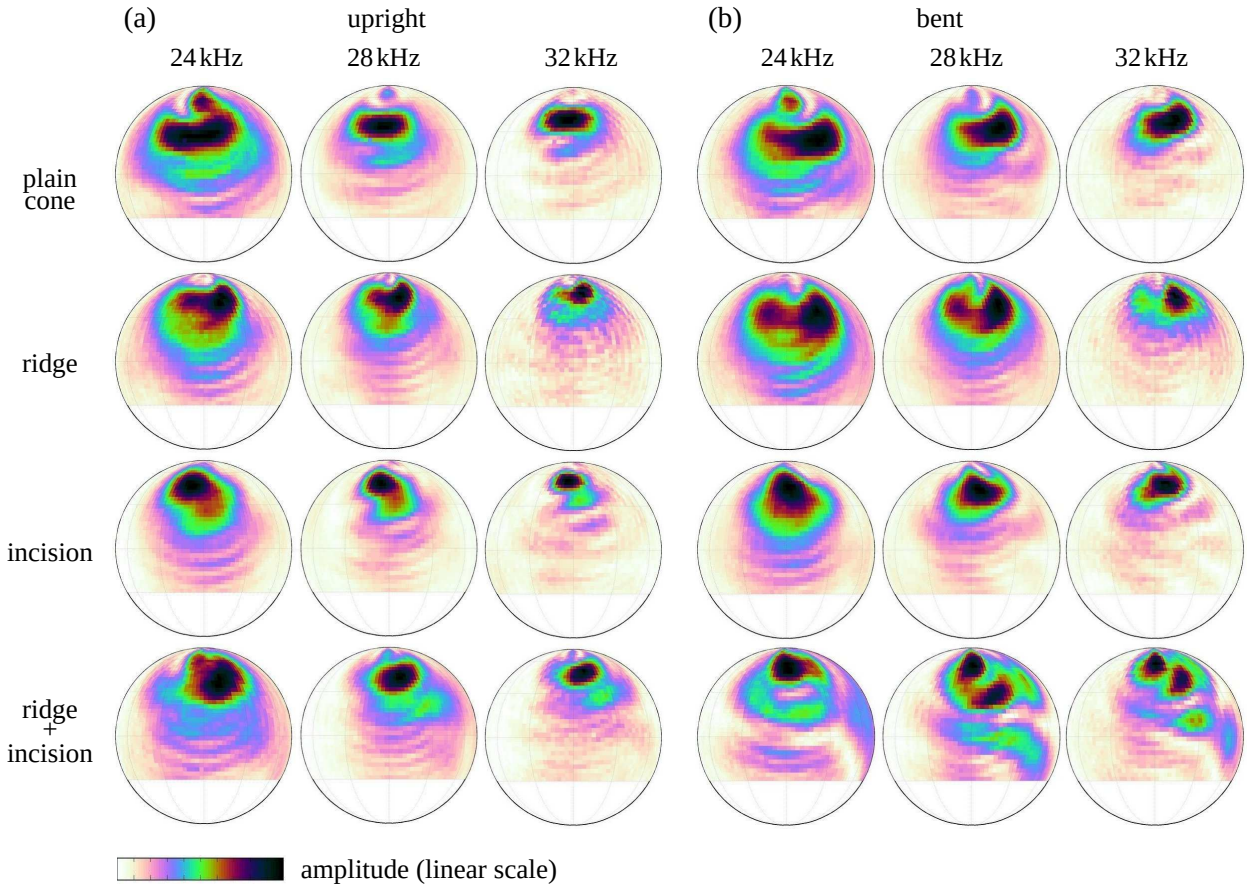

Figure 4.4: Beampatterns at upright and bent stages for cone shapes augmented with individual shape features or feature combinations: Three frequencies, 24 kHz, 28 kHzand 32 kHz for prototype corresponds to 60 kHz, 70 kHz and 80 kHz in bats, are shown for each feature combination and bending stage.

shape, in particular at the higher frequencies studied (s. Figure 4.6).

Further, multiple population t-tests with Bonferroni correction were performed by pooling this data into groups depending on the number of features in the ear prototype. Data from the ear prototype with no features was categorized into one group. Another group contained data from ears with one feature. Data from the ear prototypes with multiple features was placed into a different group.

When pooled across frequency, the data sets of amplitude-weighted sidelobe numbers showed very little evidence of differences between the plain cone and any of the three single static features with probabilities of dismissing the hypothesis that the beampatterns belong to the same population in

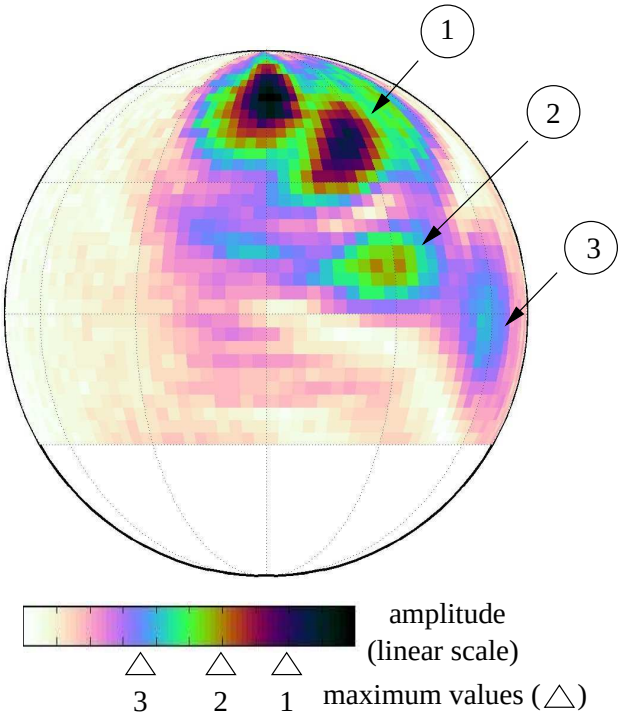

Figure 4.5: Computation of the amplitude-weighted sidelobe number from the beam gain values. The maximum amplitudes (triangles) of the sidelobes (1, 2, 3) are summed. Beam gain values are coded in gray scale from white (low values) to gray (high values). White region below -30° was not covered by the measurement

error great than 5% (s. Figure 4.7). When the amplitude-weighted sidelobe numbers for either the plain-cone or the single-feature data sets were tested against the data set associated with multiple features, the error values depended strongly on bending stage: The larger the bending stage, the smaller the error values. I.e., the beampatterns of the multi-feature shapes increasingly differed from those of the plain and single feature shapes in their amplitude-weighted sidelobes as the shape was bent (s. Figure 4.7). For the largest two bending stages, error probabilities less than 0.1% were obtained.

Similarly analysis was performed to evaluate the elevation beamwidth in the major lobes of the beampatterns. The beamwidth was calculated for all the feature combinations at every frequency along the bending stages. There was a tendency for ears with multiple features to have beams that are wider in elevation than those with single features. This tendency was clearer at higher

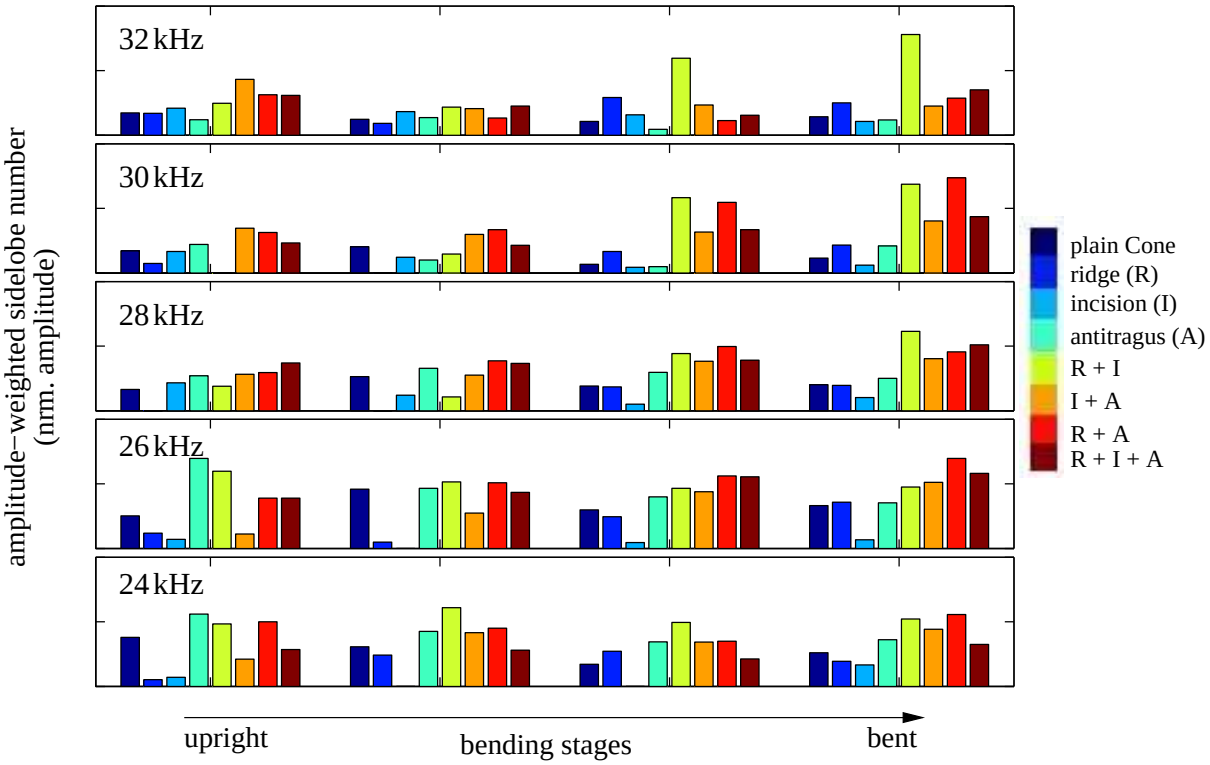

Figure 4.6: Amplitude-weighted number of sidelobes along frequencies and deformation stages. In each set of eight bar figures, from left to right-ear with no features, ear with one feature (ridge, incision, antitragus), ear with combination of features.

frequencies, but not as pronounced as the differences in the sidelobes (s. figure 4.8).

When pooling data across frequencies and the different versions of multiple and single features, results for the elevation beamwidth were qualitatively similar to those obtained for the amplitude-weighted sidelobes, but with substantially higher error probabilities for the comparisons involving multiple features (s. Figure 4.9). The probability decreased for pairings that involved multiple features as well as with bending stage; i.e. the beampatterns associated with single features never differed from those of the plain cone significantly in the elevation beamwidth , beampatterns of multiple features when compared to the plain cone differed at the 0.01 and 0.001 significance levels for the second largest and the largest bending stage respectively; the statistical significances

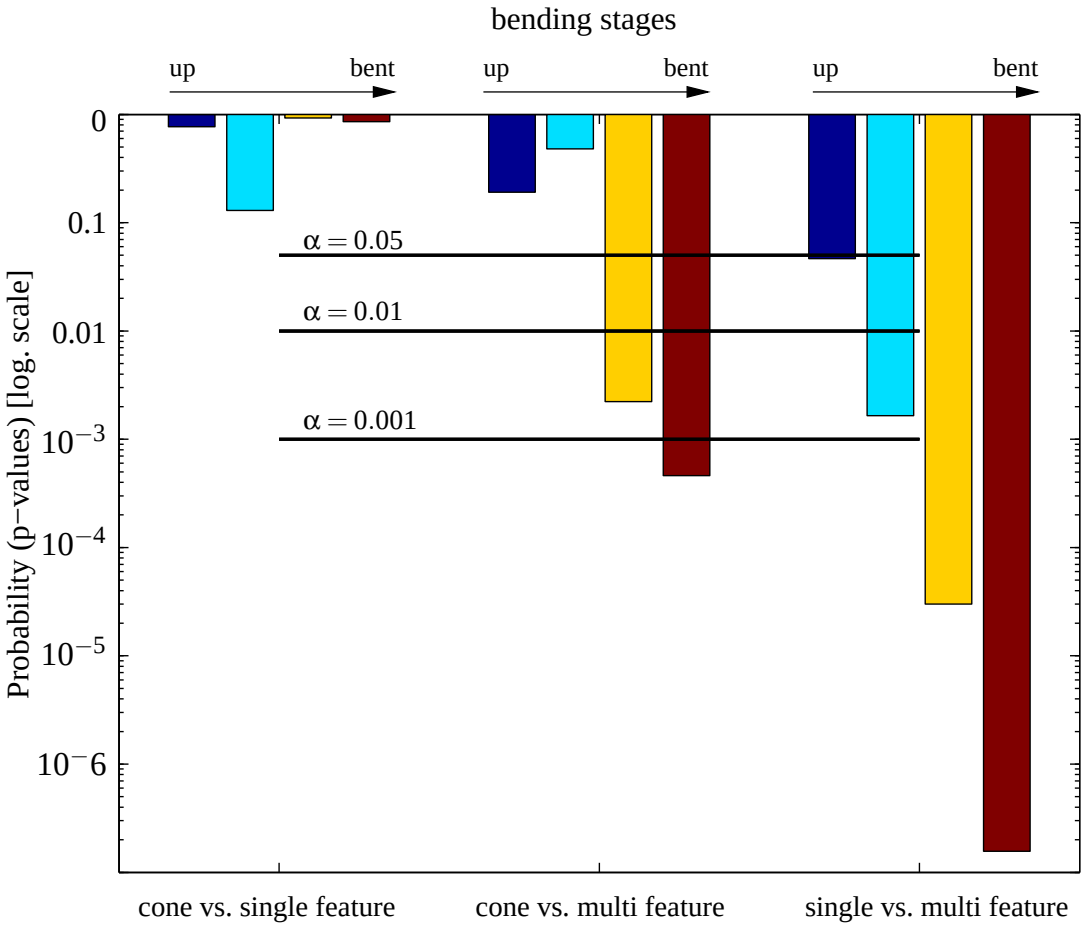

Figure 4.7: Multiple population t-tests (with Bonferroni correction) on the shape groups based on amplitude-weighted number of sidelobes. 'Cone' population consists of only plain cone data, 'single feature' population consists of data from prototypes with one feature, 'multi feature' population consists of data from prototypes with more than one feature.

followed a similar pattern for the comparisons of beampatterns caused by single vs. multiple but reached even lower error probabilities.

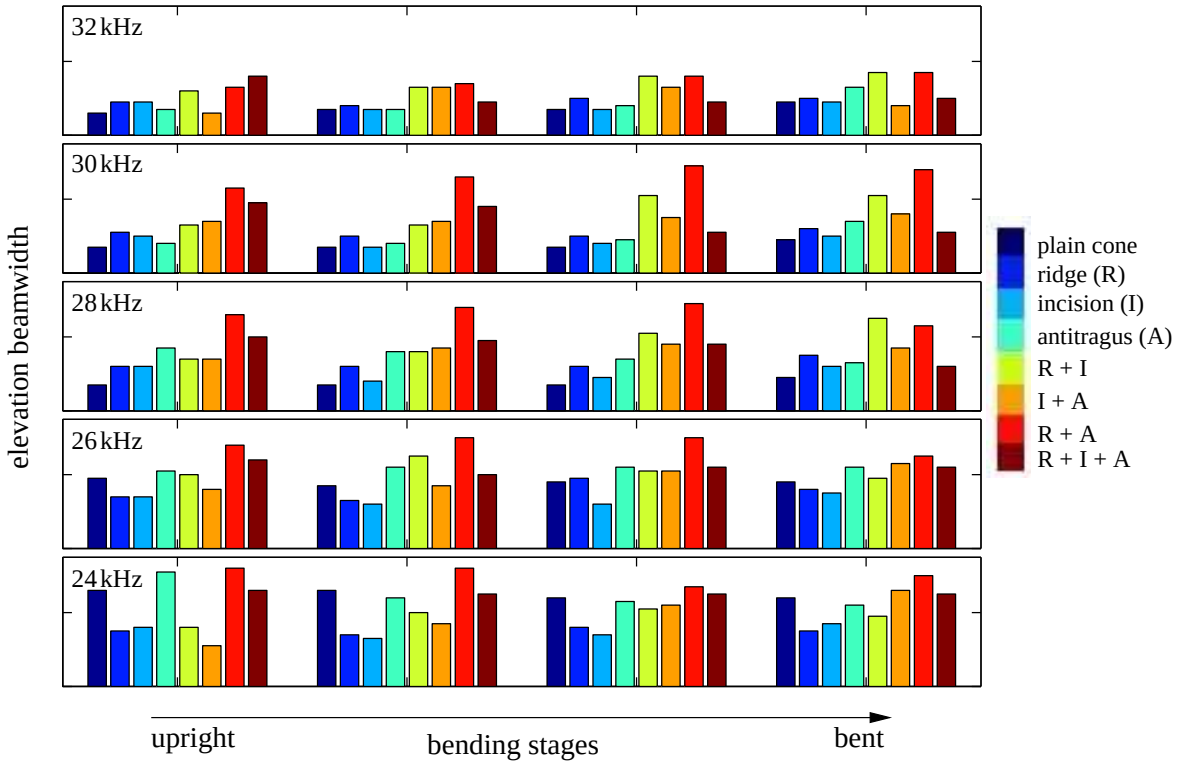

Figure 4.8: Elevation beamwidth along frequencies and deformation stages. In each set of eight bar figures, from left to right-ear with no features, ear with one feature (ridge, incision, antitragus), ear with combination of feature.

4.5 Biomimicry

The results from the dynamic change in the beampatterns as the ear prototype bends showed great qualitative similarities to the numerical beampattern estimates of the horseshoe bat deformation [39]. The beampatterns obtained through experimentation changed from one single major lobe to the formation of multiple side lobes (s. Figure 4.10). This behavior is qualitatively similar as seen in the numerical analysis of the horseshoe bat [15, 24].

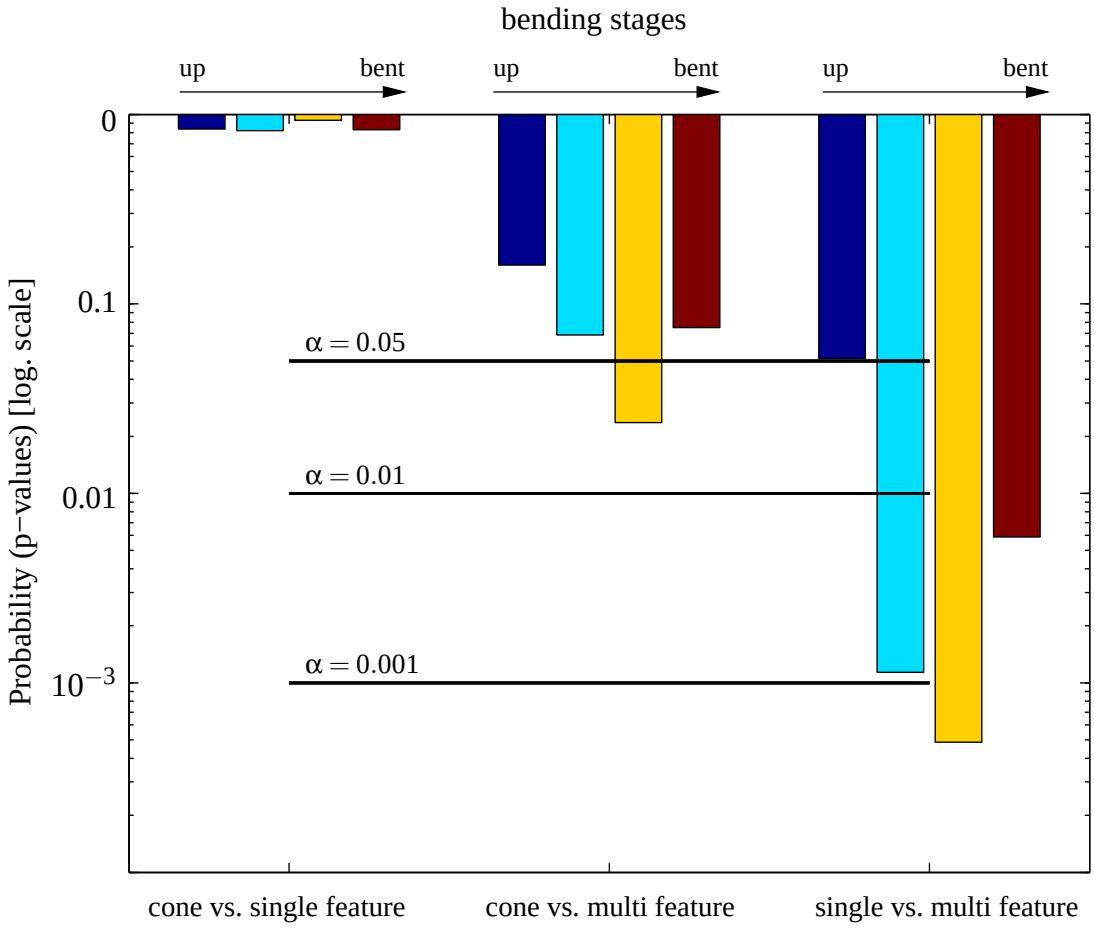

Figure 4.9: Multiple population t-tests (with Bonferroni correction) on the shape groups based on elevation beamwidth of the lobes. 'Cone' population consists of only plain cone data, 'single feature' population consists of data from prototypes with one feature, 'multi feature' population consists of data from prototypes with more than one feature.

4.6 Discussion

The biomimetic dynamic baffle prototype studied here has produced insights into the possible roles of local static features as well as dynamic changes to the overall baffle shape. As may have been expected from the relatively small size of the local shape features, adding the individual features to the plain obliquely truncated cone in isolation resulted in rather small and gradual changes to the beampatterns. The same was true for the dynamic deformations of the overall shape of the

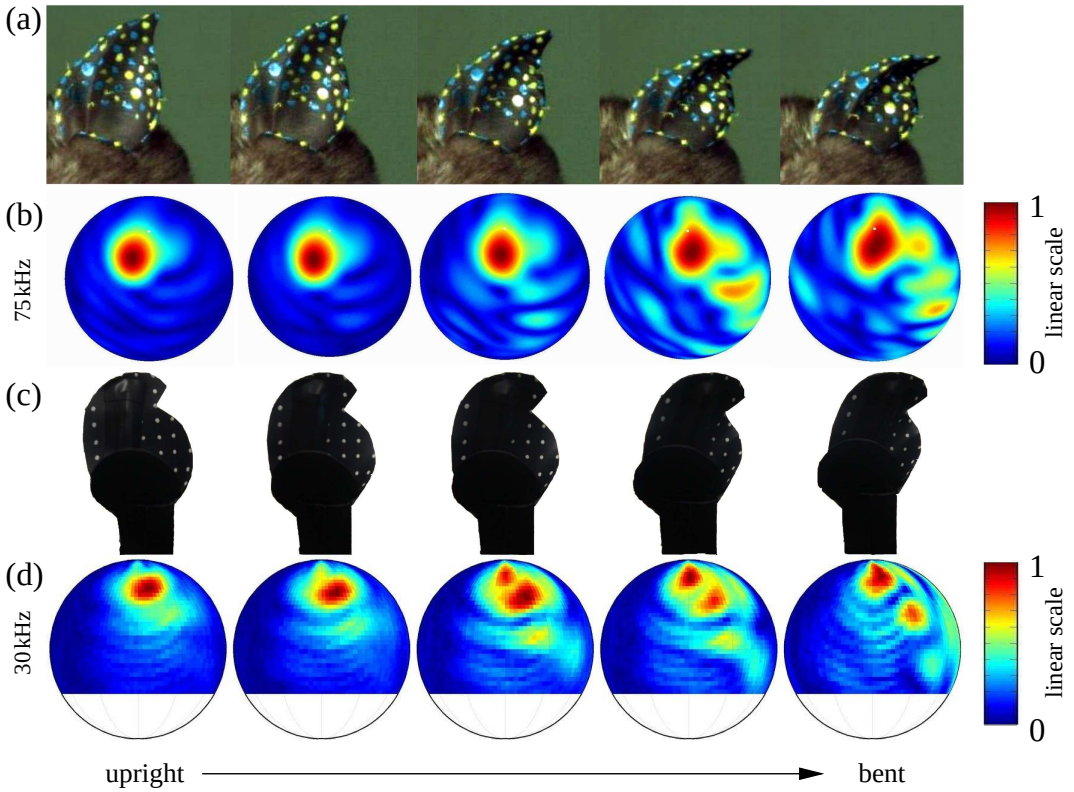

Figure 4.10: Biomimetic prototype beampattern comparisons:(a) Screenshots from a high-speed video recording of the pinna deformation in the greater horseshoe bat, (b) numerical beampattern estimates of the pinna deformation, (c) biomimetic ear prototype at different shape deformations and (d) experimental beampattern estimates for the ear prototype.

truncated cone. In the latter case, the maximum deflections amounted to about 20% of the total prototype height, but due to the elasticity of the used material, the deformations resulted in shape changes that were smoothly distributed over the shape, which could be taken as a justification for predicting the relatively minor, gradual effects on the beampattern.

In the context of these minor effects, the finding that large, qualitative changes to the beampatterns could be caused by combinations of local shape features and deformations is remarkable. Since these effects are absent when either of the involved feature is present in isolation, they must be the result of an interaction between the effects of these features. For the features studied here, bending of the overall biomimetic baffle shape generally had an amplifying effect on the effects

of the feature interactions on the beampatterns. This could be due to the fact that bending of the baffle changed the relative position as well as the orientation of the local features which could be critical to interaction effects that depend on these relationships.

The observed effects, i.e., the occurrence of frequency-dependent sidelobes when combinations of local features were present and the tip of the baffle was bent down, qualitatively matched numerical beampattern predictions derived for the shapes of deforming horseshoe bat pinnae [15]. This could be taken as an indication that the biomimetic overall baffle shape, its local shape features, and their interactions could have captured some of the functional principles of the horseshoe bat pinnae – despite their simplification. The interactions that could be readily demonstrated by comparing beampatterns across the manufactured family of prototypes, could hence serve as a hypothesis for acoustic functional effects that could be at work in the horseshoe bat pinnae.

The use of acoustic effects that rely on the interactions of local features to transform the beampattern qualitatively is an attractive proposition. The apparent sensitivity of the effects to the relative position or orientation of the local features, would provide a way to radically alter the beampattern through relatively small changes in the overall baffle geometry. At present, technical systems appear not to make use of such strategies, but they could be worth considering to make future beamforming devices more physically adaptive in a parsimonious manner.

Chapter 5

Dynamic Sensor Encoding

5.1 Introduction

Like most hearing systems in biology, bat biosonar provides information about the presence, location, and nature of sound sources in the environment [41, 42, 43]. All this information has to be encoded into the properties of the ultrasonic signals that reach the animals' tympanic membranes. The sites of ultrasound emission and reception are critical interfaces for this encoding process, because they are the locations of direction-depended acoustic diffraction. This puts them into a unique position to add informative signal components, whereas all internal stages of the hearing system are limited to removing them.

Until now, it has remained unclear if the dynamic baffle structures on the reception side, which diffract the incoming waves, result in any improvements to the horseshoe bat's pinna capacity to encode sensory information. To investigate this question, the dynamic beampattern changes obtained from the biomimetic baffles described in the previous chapters, have been used for an information-theoretical analysis to check whether any such effect can be demonstrated with physical data.

5.2 Information-theoretic analysis of biological systems

Information theoretic measures can be used to quantify the information encoding capacity of a channel regardless of the nature of the encoded information [44, 45]. Such measures have been applied to a wide range of research areas such as neuroscience, auditory signal processing, and image processing, to name a few. In neuroscience in particular, application of such methods has made significant contributions to the understanding of neural activity [45, 46]. Information theoretic methods have been used to study the encoding and decoding of stimuli-response data in both visual and auditory sensing [47]. Such studies have, for example, quantified the information contained in the neural spike trains transmitted within the visual sensing system of flies [48, 45]. Furthermore, information theoretic methods have been used to investigate various localization cues in single neurons for their coding capacity [49] as well as the information capacity and information transmission in cortical networks with neural avalanches [50].

Other applications of information theory that share certain characteristics with the problem of the work presented here are:

1. Understanding gene-expression data by finding the shared information (bits) between co-expressed gene clusters [51]

2. Quantifying 3d medical-image modalities [52]

3. Quantitative analysis of animal communications such as the song structures in humpback whales [53]

4. Clustering comparisons: to estimate which of the clustering shares the most information with all the remaining clusterings [54]

5. Providing feature selection in pattern recognition, image retrieval, bio-informatics, text classification, etc.

Information theoretic measures were performed to estimate the target localization accuracy in bat

biosonar [34, 55]. Although source localization in azimuth plane was estimated using head-related impulse responses [56], so far, the coding capacity in head-related impulse responses/head-related transfer functions (HRTFs) has not been investigated. The work presented in this chapter aims at understanding the sensor coding capacity in the dynamic deformation of the bat's baffle structure.

5.3 Coding capacity of the biomimetic pinnae

Entropy is a measure that can be used to quantify the capacity of a channel for carrying information [57]. It cannot be used to determine the amount of information that is actually evaluated or the nature of the information that is conveyed. I.e., entropy provides an upper bound for the amount of information that could be passed through a channel. In the case of the present work, this channel is the biomimetic reproduction of the bat pinna. Here, the entropy refers to information-theoretic measure which is different from the thermodynamic measure of entropy.

For a random variable x that can take on N discrete values, entropy $H(x)$ is defined as [58, 44]

$$H(x) = -\sum_{x=1}^{N} P_x \log_2(P_x), \tag{5.1}$$

where P_x is the probability of the occurrence of a certain value of x in the sample population. The entropy can hence be viewed as the amount of uncertainty in the random variable.

To determine the dynamic encoding capacity across two shape configurations of the biomimetic pinna, joint entropy can be estimated. The joint entropy quantifies the uncertainty contained in the joint system of the two variables. It can be taken as a quantification of the coding capacity of the system with two variables.

For two discrete random variables x and y with N different values, joint entropy is given by [44]

$$H(x, y) = -\sum_{x=1}^{N}\sum_{y=1}^{N} P_{xy} \log_2(P_{xy}), \tag{5.2}$$

where P_{xy} is the joint probability distribution of the two variables.

If some form of dependence exists between the two random variables, their joint entropy will be less than the sum of their individual entropies. The difference between the sum of the individual entropies and the joint entropy hence represent the amount of shared information and is known as the mutual information (MI). It measures the reduction in uncertainty in x when y is known. In other words, the MI evaluates the relationship between the two random variables by providing a measure of the dependencies between them. In this sense, mutual information can be seen as a generalization of correlation. Whereas correlation quantifies a linear relationship between variables, the MI is capable of capturing non-linear relationships. The MI $I(x, y)$ is defined as [44]

$$I(x,y) = \sum_{x=1}^{N} \sum_{y=1}^{N} P_{xy} \log_2 \frac{P_{xy}}{P_x P_y}, \tag{5.3}$$

where P_x and P_y are the marginal probabilities of the random variables x and y and P_{xy} is the joint probability distribution. MI can also be obtained as the sum of entropies of x and y minus the joint entropy.

$$I(x,y) = H(x) + H(y) - H(x,y) \tag{5.4}$$

For all the equations defined above, the logarithm has the base two and hence entropy and mutual information are measured in units of bits.

Signal data that was experimentally acquired using the biomimetic prototype was used for analyzing the coding capacity. As explained in chapter three, signals were recorded at each of 2,501 directions spanning -90° to +90° in azimuth direction and -30° to +90° in the elevation direction with a spacing of 3°. In order to use this time series data for quantification of coding capacity, spectral clustering techniques [59] were applied to group the data into certain alphabet classes.

Using Fourier transforms, transfer functions were obtained from the time-series data of the measured responses. These functions vary significantly in the direction space due to the incoming sound diffracting from the surface of the baffle structure (s. Figure 5.1). For finding alphabet classes, amplitude gain values at 129 frequencies in the range from 24 kHz to 32 kHz in the trans-

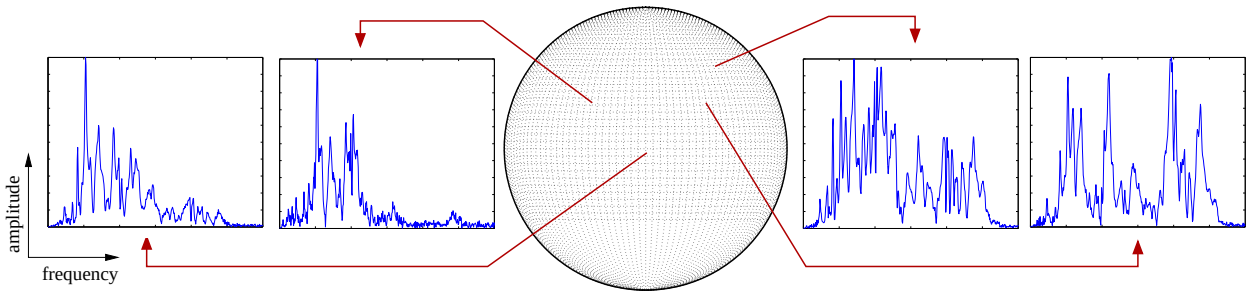

Figure 5.1: Example transfer functions for four positions in the directivity space (linear scale)

fer function were found. All the 129 beampatterns for each bending stage were used to group into discrete alphabet classes using spectral clustering algorithms (see below).

5.4 Spectral clustering

Before applying clustering methods, the variability in the 129 dimensions was investigated by performing principal component analysis (PCA). Only 33 dimensions show variability and the remaining eigen values were zero (s. Figure 5.2).

A Gaussian similarity function was applied to these 33 principal components to obtain a fully connected graph, represented in the form of a similarity matrix, where the edges connecting the data points (vertices) are the elements of the matrix. This matrix was formulated for all the positions in the seven bending stages resulting in 17,507 element $(2, 501 \times 7)$ square matrix. A PCA of the similarity matrix was followed by k-means clustering, on the transformed similarity matrix to assign each transfer function to a cluster, i.e., a "character" in the discrete alphabet. In this way, a cluster number was obtained for every position (data point) in the direction space. The first k eigenvectors calculated from the spectral clustering techniques constituted k classes. These discrete transfer function identifiers were used for the information-theoretic analysis.

For the clustered transfer function data analyzed here, the marginal and joint probability densities in Eqs. 5.1, 5.2 and 5.3 were carried out across bending stages of the biomimetic prototype. The samples of the two discrete random variables x and y were each represented by vectors of cluster

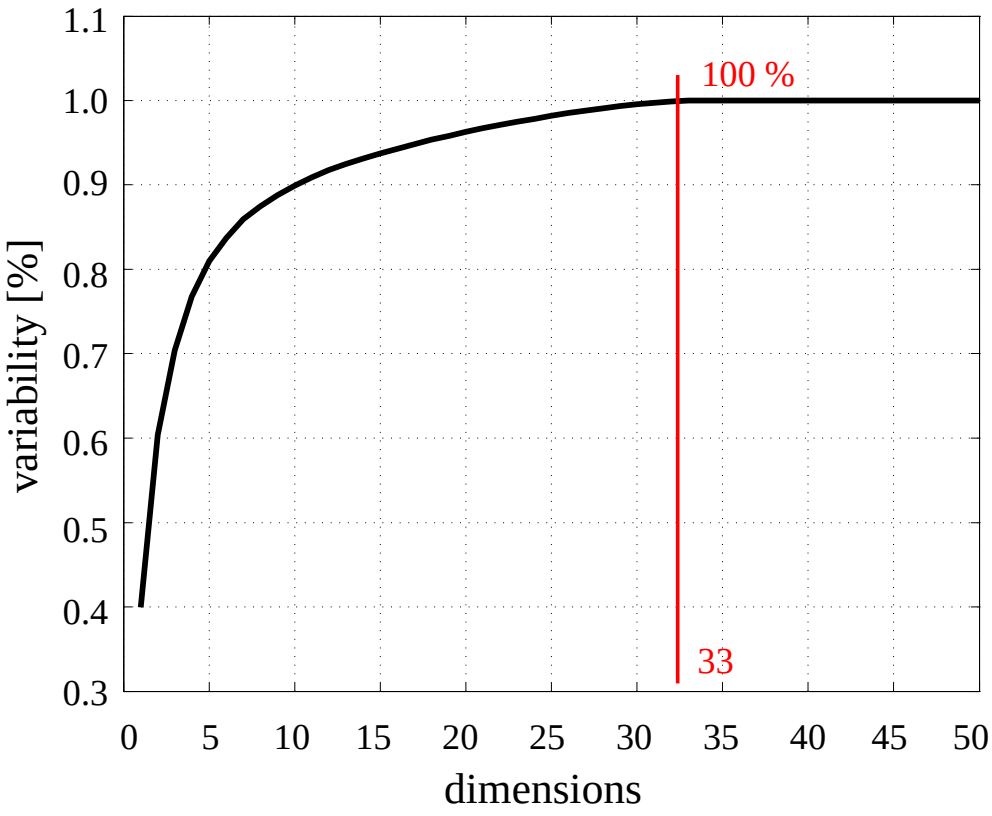

Figure 5.2: 100 % variability found in 33 of the 129 dimensions. Only 50 dimensions are shown on the x-axis

identities across all 2,501 positions sampled in the direction space.

5.5 Sampling bias corrections

For finite sample sizes, the estimates of marginal and joint probabilities contain errors and as a consequence, the estimated entropy and mutual information values are biased. Since the sample size for each bending stage was comparatively small (2,501 points), bias corrections were required.

Various estimates for biases have been derived depending on whether the variables are continuous or discrete in nature [60, 61, 62, 63, 64] and new techniques for bias correction for these measures continue to be developed [65].

The bias corrections applied for marginal and joint entropies in the current work were [53]

$$\text{Bias}\{H(x)\} = 0.72 \times \frac{D-1}{N} \tag{5.5}$$

and

$$\text{Bias}\{H(x,y)\} = 0.72 \times \frac{B-K}{N}, \tag{5.6}$$

where D is number of nonzero marginal probabilities, B is the number of nonzero joint probabilities for K alphabet sizes (number of clusters) and N is the total number of samples.

Since entropy measures the variability in the data, when the sample size is finite, variability measured in the data is lower than the true value with infinite samples. This leads to negatively biased or underestimated entropy. Therefore Bias$\{H(x)\}$ is added to the estimated entropy to improve the estimate by reducing its bias.

The bias correction applied for mutual information estimate is [64].

$$\text{Bias}\{I(x,y)\} = \frac{B}{2N\log_e(2)}, \tag{5.7}$$

where B is the number of nonzero joint probability values and N is the number of samples.

Due to finite sampling, mutual information is positively biased or overly estimated and the bias correction: Bias$\{I(x,y)\}$ is subtracted from the estimated value to reduce the bias.

The mutual information estimates thus obtained appeared to depend systematically on alphabet size. With increase in alphabet size, the mutual information always increased. However, for very high alphabet sizes, mutual information must decrease to zero. Thus optimum alphabet size needs to be determined. This can be considered similar in concept to estimating the right number of bin sizes for Gaussian distribution. Very high and very low number of bins will incorrectly estimate the Gaussian distribution (s. Appendix A).

5.6 Permutation test

To estimate the optimum alphabet size, permutation tests were performed. This test was chosen since mutual information is a measure of the similarity between two variables. For this test, the data from each pairwise comparison of beampattern clusters were shuffled and re-assigned randomly to the two bending stages. This reshuffling of the data preserved the frequency of the different class identities, but disrupted any dependencies between the two variables. Hence, MI values obtained for this reshuffled data sets will be estimates of the bias. To obtain these bias estimates, fifteen such permutations were carried out and the MI was evaluated. The mean value of the permuted MI was taken as an estimate of the bias and subtracted from the MI estimates obtained for the original data set to obtain corrected estimates. As a validation for this approach, the same method was performed on two continuous Gaussian variables with known dependencies (s. Appendix B).

5.7 Results

When the similarity matrices were decomposed using PCA, the first eigenvalue was found to be zero and the subsequent eigenvalues obtained were of approximately equal size. This can be seen as an indication that the clustering was splitting a continuum of transfer functions rather than following discontinuities already existing in the data. Nevertheless, the resulting clusters showed non-random spatial patterns over direction (s. Figure 5.3). Since no direction information had been included in the clustering, these non-random spatial patterns can be taken as evidence that the elements of the alphabet represented deterministic directional trends existing in the transfer function data rather than some form of random noise.

The beampattern entropy estimates for the different studied alphabet sizes (2 to 10 elements) were used as measures for the coding capacity of the beampatterns in a manner similar to previous research on whale songs [53] and neural coding [50, 47]. For each of the studied alphabet sizes, the entropy estimates obtained were close to the maximum possible entropy for the respective alphabet

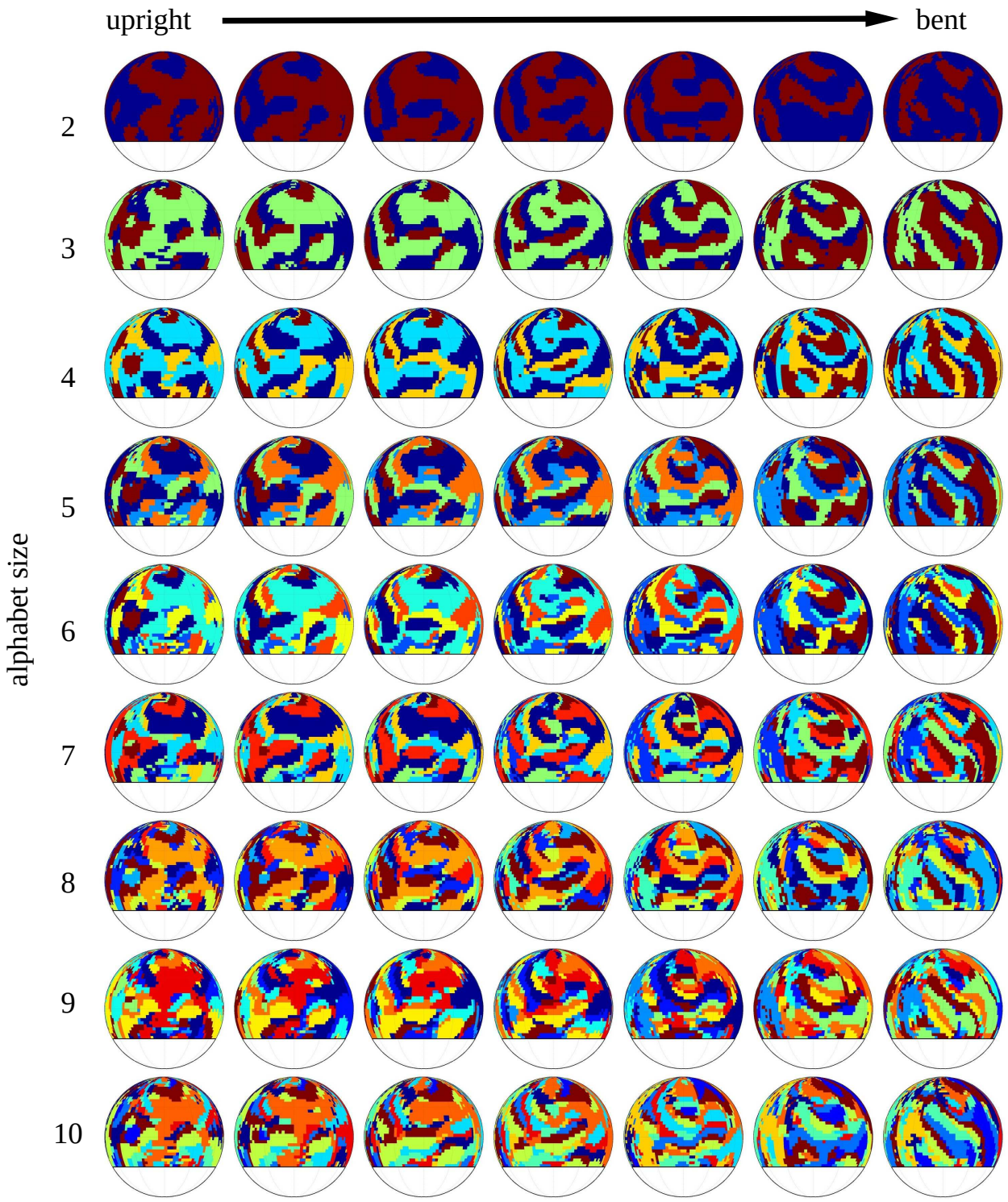

Figure 5.3: Clustering of beampatterns of different bending stages into discrete alphabets based on spectral clustering applied to transfer function vectors. Columns indicate alphabet sizes of two (top) to ten (bottom). Color codes for the different elements of the alphabet.

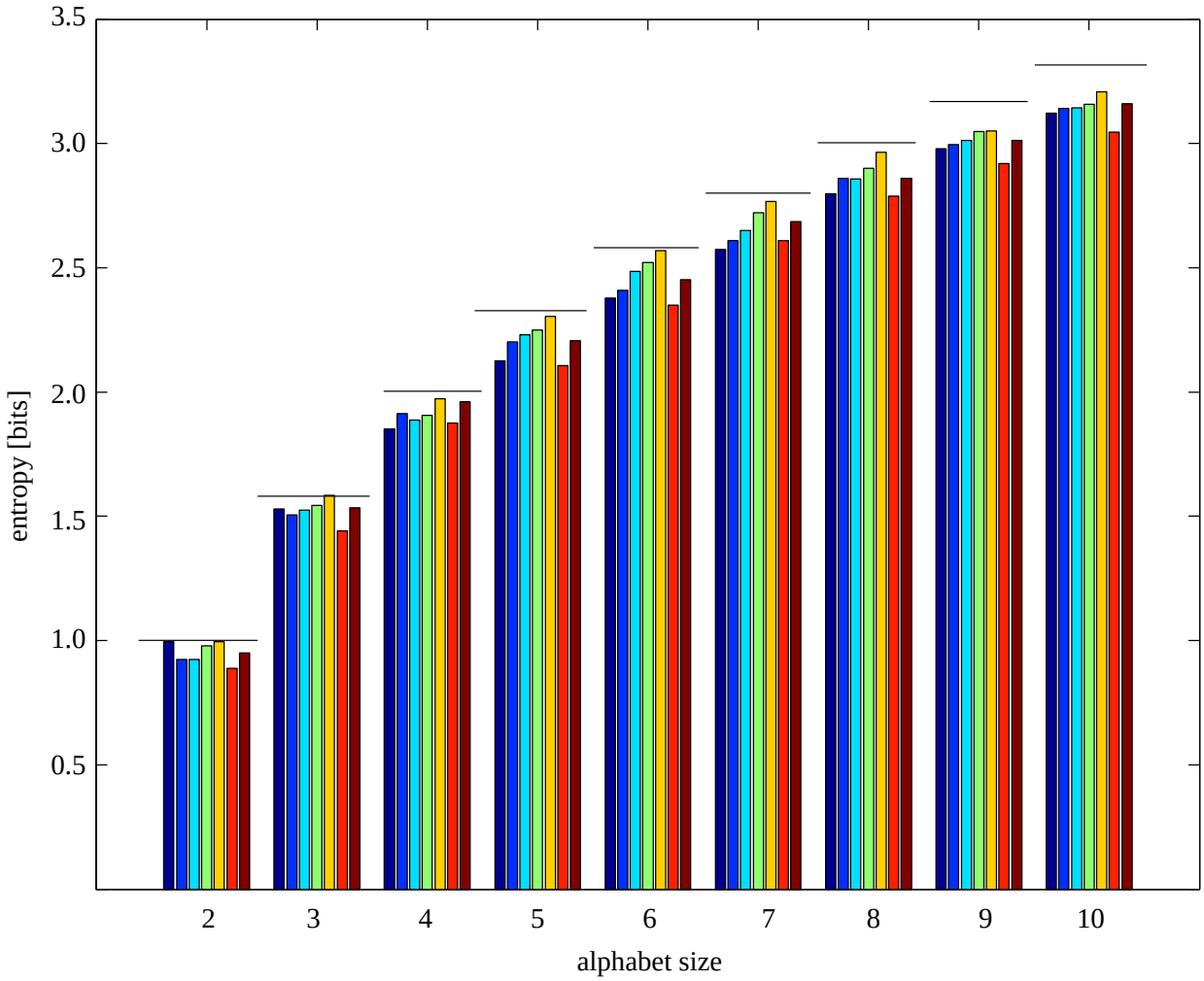

Figure 5.4: Entropy estimates for the discretized beampatterns as a function of alphabet size. The different bars in the groups for each alphabet size represent the different bending states of the biomimetic device from upright (blue) to bent (red). The horizontal bar over each group indicates the maximum entropy that is possible for the respective alphabet size ($H_{\max} = \log_2 |A|$, where A is the alphabet size [53]).

size (s. Figure 5.4). As a consequence, estimated entropies traced the increase in maximum entropy with alphabet size. For any tested alphabet size, entropy was found to be largely unaffected by the bending stage of the biomimetic device, i.e., no matter what bending stage the baffle was in, the entropy in the transfer function alphabet was always close to the theoretical maximum (s. Figure 5.4). This suggests that there is a significant encoding capacity in the beampatterns that appears not to be affected by the bending stage of the device.

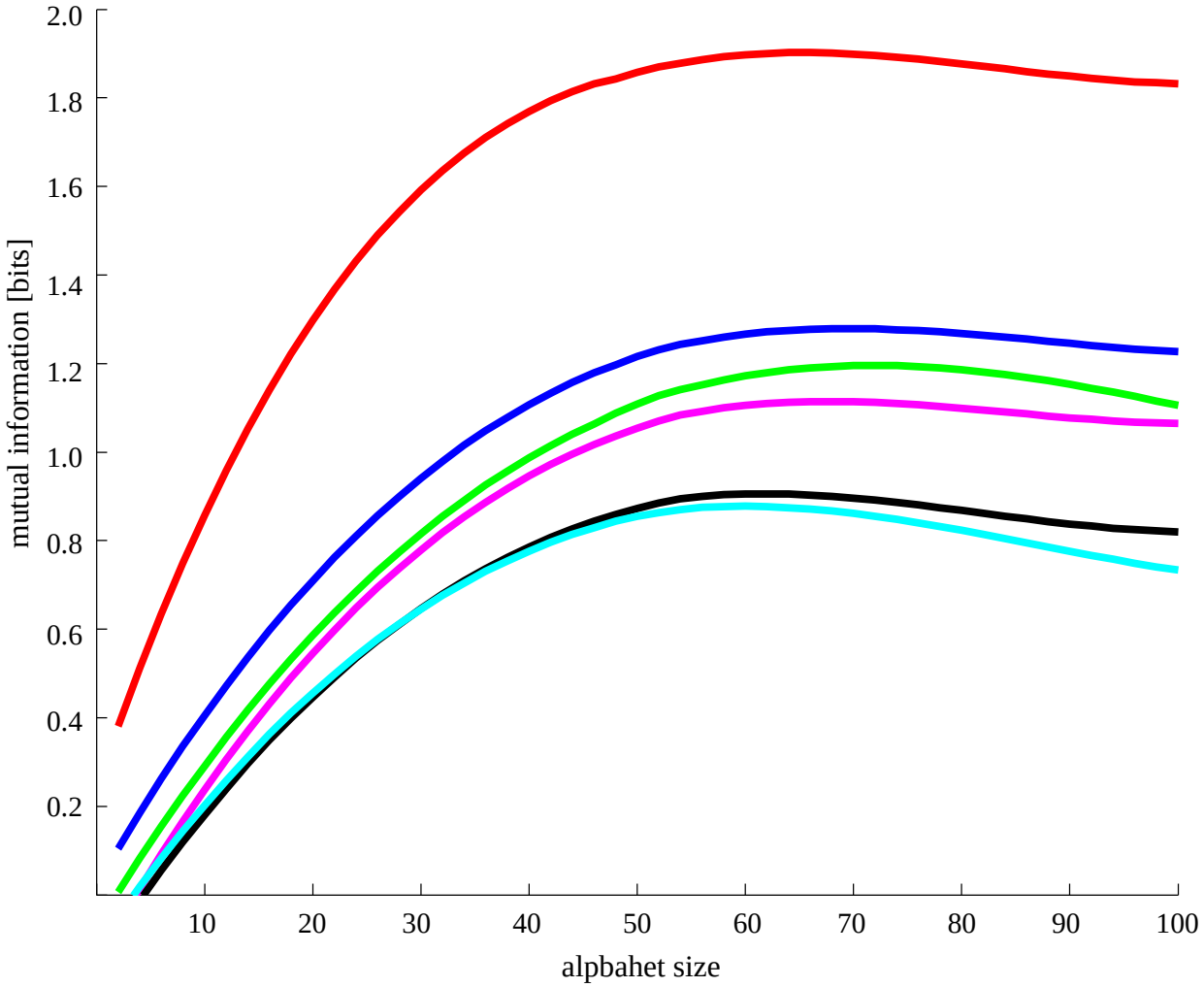

Figure 5.5: Mutual information reaches maximum and then decays to zero with increase in alphabet size. Up to 100 clusters are shown here. The colors represent different bending stages - red, blue, green, magenta, black and cyan in order indicate upright to bent stages.

With increase in alphabet size, the mutual information estimates increased to a maximum and then reduces to zero at alphabet sizes of 500 and higher. The mutual information curves were smoothed using Savitzky-Golay filters [66] with cubic polynomial curves. The maximum for the mutual information occurred at alphabet sizes between 60 and 72 clusters for different bending stages. (s. Figure 5.5).

The maximum mutual information normalized with the joint entropy was found to decrease monotonically with the distance of the compared stages within the deformation sequence (s. Figure 5.6).

For one step size of sampling the bending in which the baffle tip moved by about 20 % of the total device height of 5 cm, mutual information decreased to about 20%. The normalized mutual information between the beampatterns at the end points of bending sequence was around 10%.

Here the mutual information has been normalized with the joint entropy estimates that were obtained for the same alphabet size as the mutual information. However, the permutation method that was used to estimate the bias in the MI estimates is not applicable to the joint entropy estimates and hence it is not certain that the best alphabet size for the joint entropy estimates equals that for the mutual information.

The increase in coding capacity was also quantified by estimating joint beampattern entropies across an increasing number of bending stages (s. Figure 5.7): For the alphabet size where maximum mutual information was found, the joint entropy increased with alphabet size and saturated for alphabet sizes of much higher value. Furthermore, the joint entropy also increased with the addition of bending stages. Whereas the entropy of the beampatterns associated with the upright pinna was only around one to three bits (depending on alphabet size, Figure 5.4), the joint beampattern entropy for all seven bending stages increased to values between 5 and 10 bits, i.e., by factors between three and five.

5.8 Discussion

The results presented here for a biomimetic baffle modeled after the pinna of horseshoe bats have demonstrated that dynamic shape changes similar to the ones observed in the animals increase information encoding capacity. Together with the muscular specializations in horseshoe bats [19] as well as in the related Old World leaf-nosed bats (*Hipposideridae*) [67, 68] and the prominence of these deformations in the biosonar behavior of the animals, these findings constitute a significant further piece of evidence in favor of the hypothesis that the dynamics of the noseleaves and pinna shapes in bats is an active sensing behavior. According to this hypothesis, horseshoe bats – and perhaps other species with similar behaviors – would use dynamic shape changes of their nose-

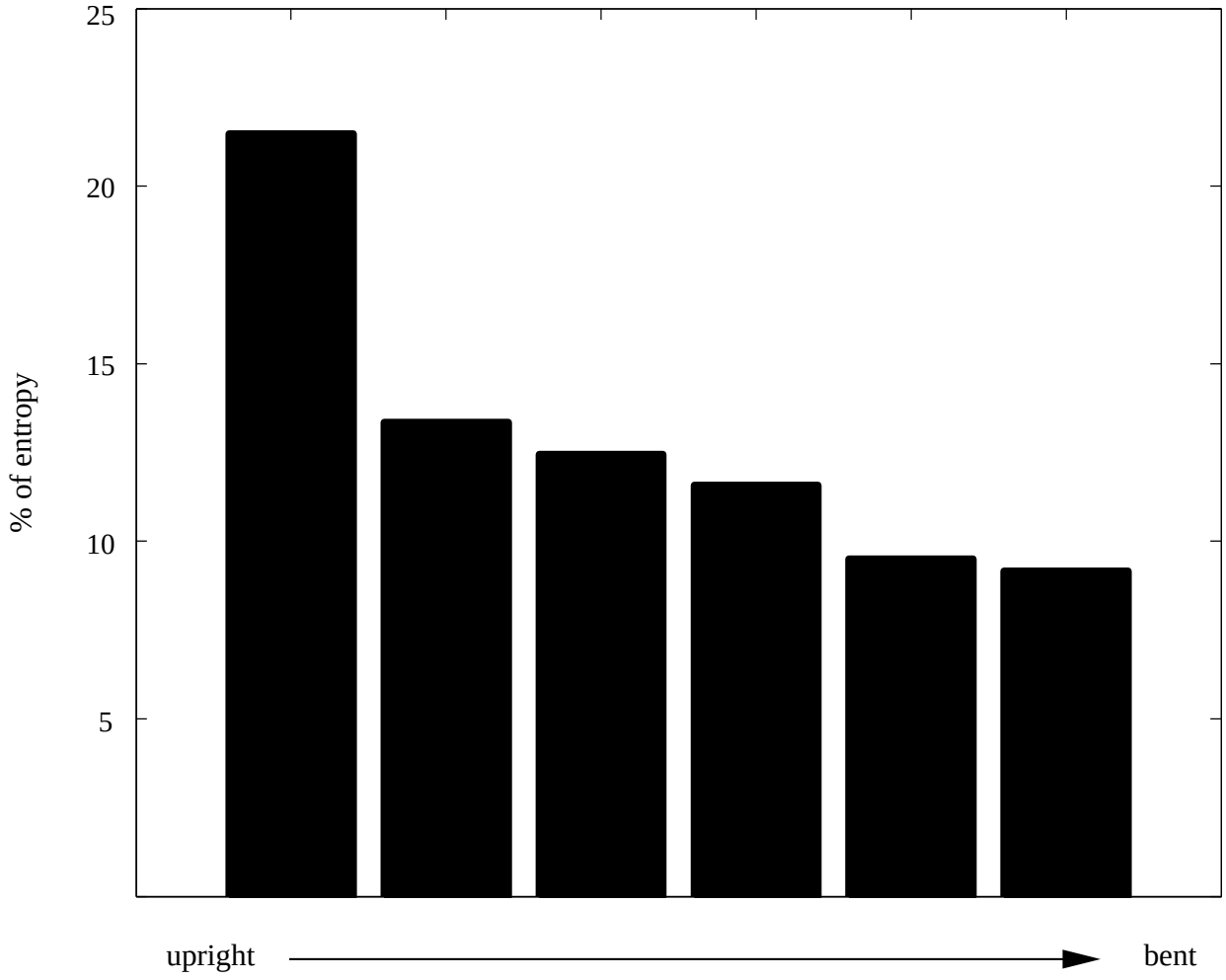

Figure 5.6: Increase in encoding capacity over the bending sequence of the biomimetic prototype as normalized mutual information between the discretized beampattern of the upright baffle shape compared to successive bending stages decreases.

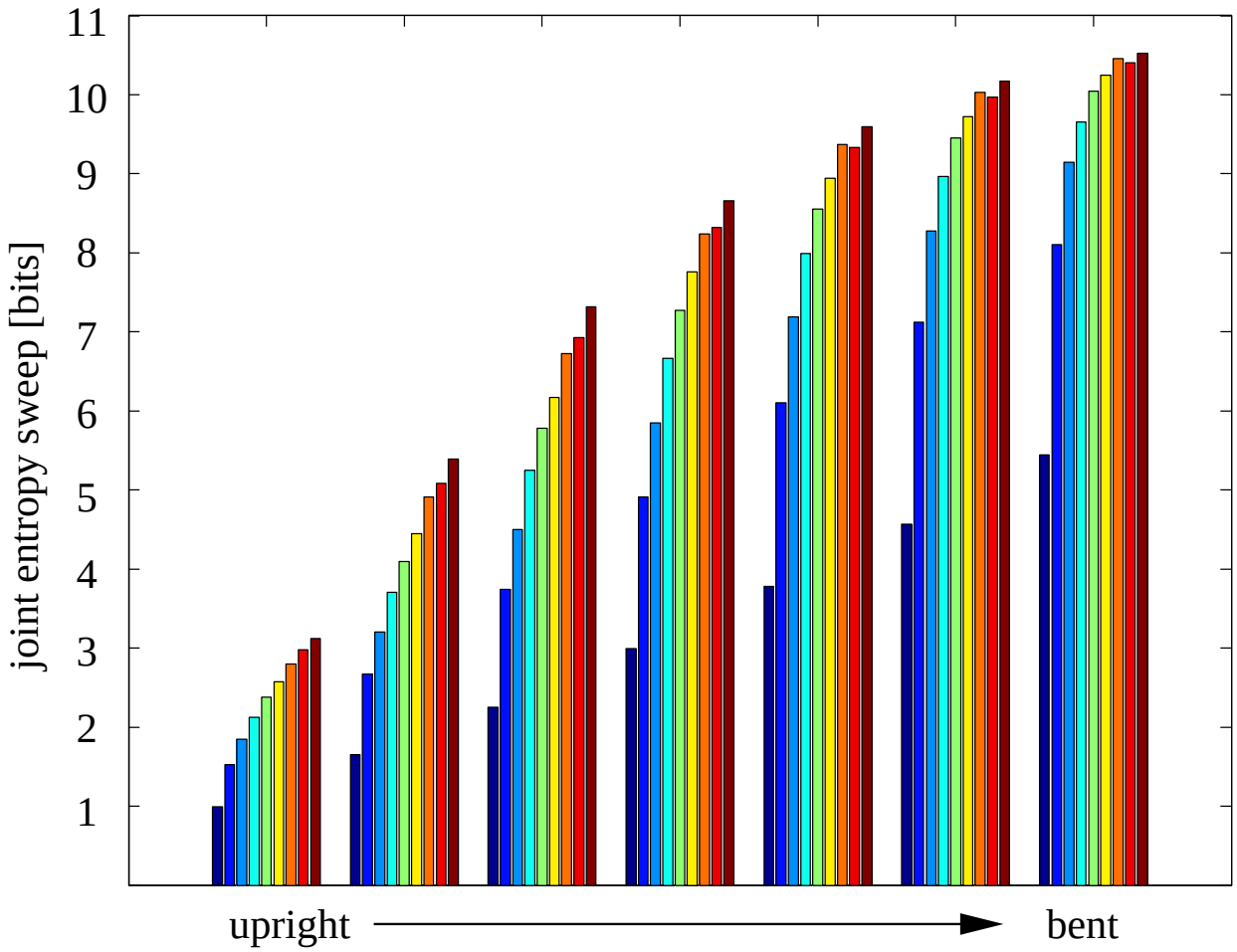

Figure 5.7: Increase in encoding capacity over the bending sequence of the biomimetic prototype: joint entropy across the different bending stages studied. Individual bars in the groups correspond to the different discrete alphabet sizes from two (blue) to ten (red).

leaves and pinnae to enhance the capacity of their auditory periphery, i.e., a critical interface with the external world, to encode biosonar information. At present, it remains unknown whether this coding capacity is actually used in nature and if this is the case what information is encoded with it. However, if this could be determined, the dynamics of biosonar systems could become a paragon for novel, dynamic sensing paradigms that would not only be new to the study of biological sensing systems but also to engineering. These strategies could provide ways in which critical bottlenecks in the ability of sensory systems to encode information with sufficient quantity and quality could be eliminated. Such insights could lead to a deeper understanding of sensing in nature as well as to novel sensing technologies.

Chapter 6

Summary

6.1 Research accomplishments

In the course of the research work presented in this dissertation, the following major research accomplishments were made:

1. Developed a simple and parsimonious biomimetic baffle structure mimicking the pinna of greater horseshoe bat.
2. The actuation mechanism used in this work was able to deform the biomimetic prototype by mimicking the bat ear deformation.
3. Three local shape features were identified, which play a vital role in the formation of acoustic beampatterns.
4. The biomimetic prototype was able to mimic the beampattern changes as seen in the numerical simulation of the horseshoe bat.
5. Beampattern data obtained from this experimental setup was used to understand the sensory coding capacity of the dynamic deformation. It was found that the bat can increase its coding capacity by deforming the ear.

6. A novel technique was explored: Information theoretical analysis for dynamic sensory coding capacity using head related transfer functions.

6.2 Major findings

The following major findings have resulted from the work presented in this dissertation:

1. The static and dynamic effects of three local shape features namely, ridge, incision and antitragus of the greater horseshoe bat pinna were investigated. It was found that each of the individual features studied here effected only small, gradual changes in the beampatterns by itself. In contrast to this, several combinations of multiple features did result in large and qualitative changes to the beampatterns. This can be taken as evidence for an interaction between the acoustic diffraction effects of these features.

   This notion is reinforced by the findings of quantitative differences between multiple-feature beampatterns and single-feature even greater than those between the plain cone-beampattern and the multiple-feature beampatterns - this result indicates that the effects of feature-combinations on the beampatterns take a different direction than those associated with the individual features [25].

   The bend configuration led to greater changes in the beampatterns and presumably more interactions between the static features. Hence, there were interactions not only between the individual static shape features, but also between the static features and the dynamics of the prototype shape.

2. The effects on the beampatterns were similar to those observed in the beampattern predictions of real horseshoe bat ears, where combinations of multiple features and bending tended to produce strong sidelobes [39].

3. The biomimetic prototype can encode additional sensory information with dynamic shape changes. This can be taken as a evidence supporting our hypothesis of the bat's coding

capacity through its deformable baffle structures. Although, the joint entropy presented in this work is uncorrected for alphabet sizes, assuming an increase of the mutual information by 100 % to 40 % due to change in joint entropy, our hypothesis of the coding capacity of the bat's pinna could still be supported due to 60 % change of information.

6.3 Suggestions for future work

1. The biomimetic prototype developed here is a simple and parsimonious model. Automated and more sophisticated shape changing antennas can be developed.

2. Dynamic Characterization

   The dynamic behavior of the biomimetic prototype(plain cone) was characterized using four different variables: Two variables for direction (azimuth and elevation) and two variables representing the time-variant response [40]. The impulse response of the system across direction as a function of deformation time and time delay was visualized in the time-direction domain. Qualitative changes were observed in patterns over time delay. Although, there were very slight changes at the initial, with increasing time delay clearer patterns were observed with deformation (s. Figure 6.1).

   In the delay-time domain visualization (s. Figure 6.2), two directional impulse response as a function of deformation time and time delay were mapped for a point in direction space. The initial phase of the impulse response (typically $\sim$25 µs) caused very slight changes over most of the direction space and during deformation. But the remaining part of the impulse response, showed significant differences with bending.

   Such characterizations can be performed to observe the effects of the local shape features.

3. Finally, better bias correction methods could be derived and applied to the estimation of the information theoretic measures for coding capacity.

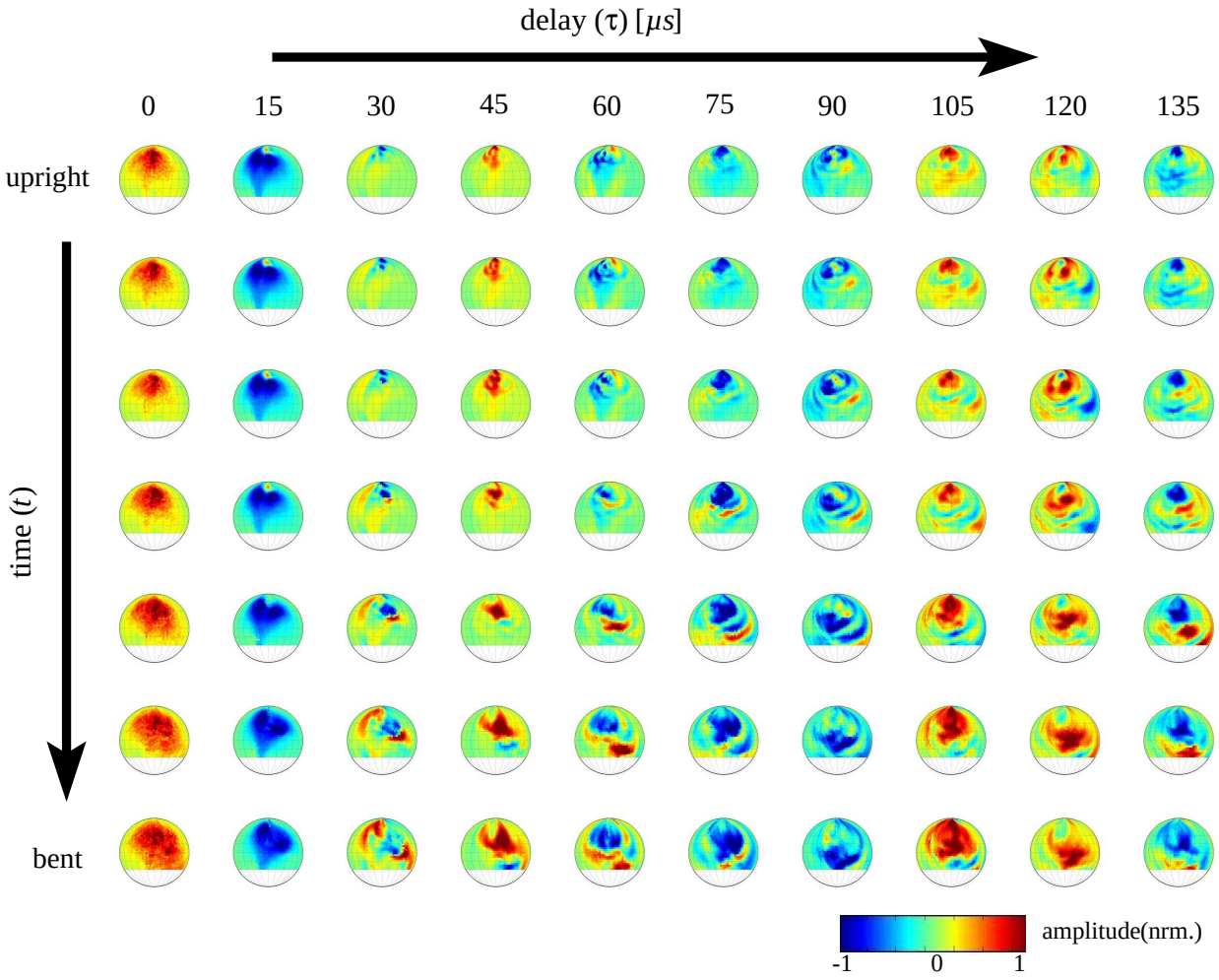

Figure 6.1: Characterization in the time-direction domain: impulse response amplitude as a function of time in the deformation cycle (rows) and time delay (columns). Colored version of the figure reproduced from [40]. See page 10 of copyright permissions document.

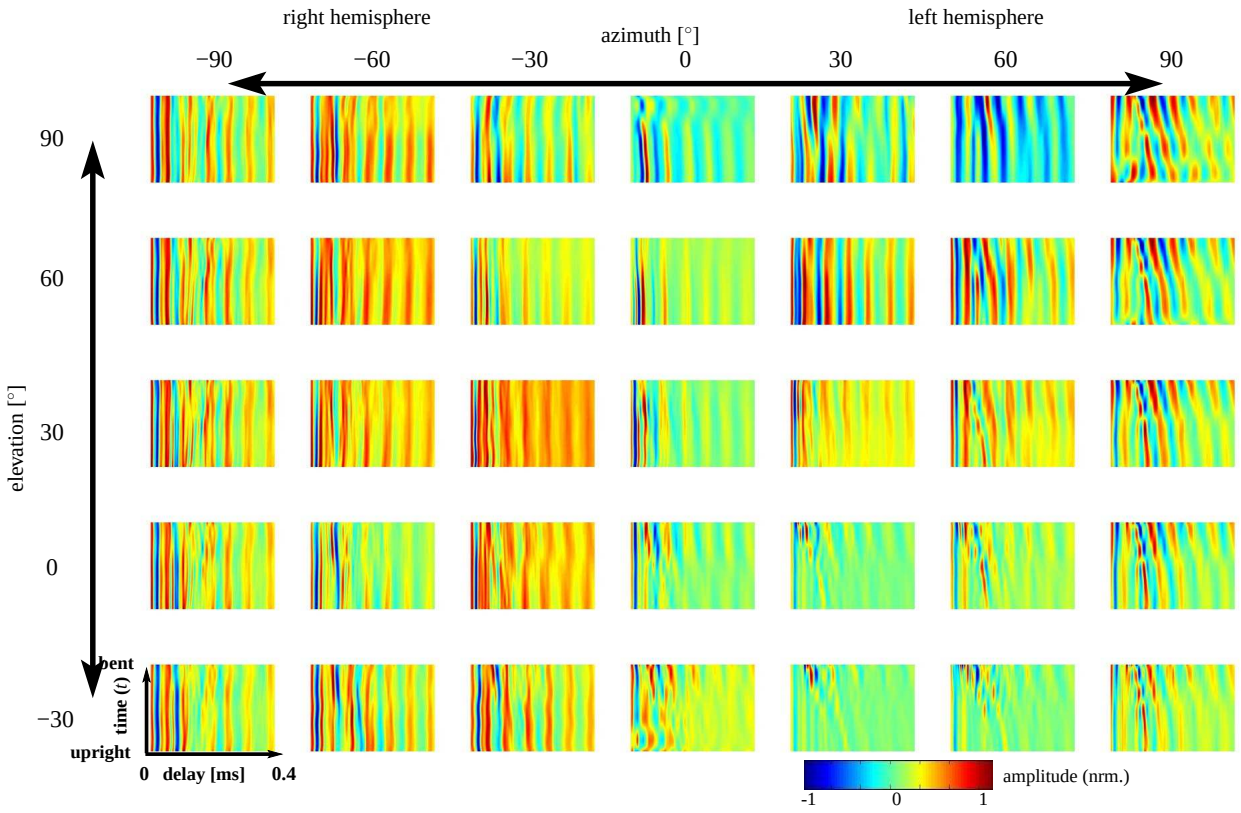

Figure 6.2: Characterization in the delay-time domain. Colored version of the figure reproduced from [40]. See page 10 of copyright permissions document.

Bibliography

[1] Vincent J F, Bogatyreva O A, Bogatyrev N R, Bowyer A A, and Pahl A K. Biomimetics: its practice and theory. *J. Roy. Soc. Interface*, 3(9):471–482, 2006.

[2] Budde R. The story of velcro. *Phys. World.*, 8:22–23, 1995.

[3] Lyon R F. The optical mouse. Technical report, Xerox Corporation, Palo Alto, CA, 1981.

[4] Hayward B and Davis R. Flight speeds in western bats. *J. Mammalogy*, 45:236–242, 1964.

[5] Simmons N B. *Mammal Species of the World: A Taxonomic and Geographic Reference*, volume 1, chapter Order Chiroptera, pages 312–529. Johns Hopkins University Press, Baltimore, MD, 3rd edition, 2005.

[6] Fenton M B. *Just Bats*. University of Toronto Press, Toronto and Buffalo, 1983.

[7] Neuweiler G. *Biology of Bats*. Oxford University Press, New York, USA, 2000.

[8] Hill J E and Smith J D. *Bats: A Natural History*. University of Texas Press, Austin, 1984.

[9] Ryan M J, Tuttle M D, and Barclay R M R. Behavioral responses of the frog-eating bat, trachops cirrhosus, to sonic frequencies. *J. Comp. Physiol. A*, 150(4):413–418, 1983.

[10] Jones G and Teeling E C. The evolution of echolocation in bats. *Trends Ecol. Evol.*, 21(3):149–56, Mar 2006.

[11] Kober R and Schnitzler H-U. Information in sonar echoes of fluttering insects available for echolocating bats. *J. Acoust. Soc. Am.*, 87:882–896, 1990.

[12] Ma J and Müller R. A method for characterizing the biodiversity in bat pinnae as a basis for engineering analysis. *Bioinspir. Biomim.*, 6(2):026008 (12pp), June 2011. (featured article).

[13] Müller R. Numerical analysis of biosonar beamforming mechanisms and strategies in bats. *J. Acoust. Soc. Am.*, 128(3):1414–1425, September 2010.

[14] Pedersen S and Müller R. *Bat Evolution, Ecology, and Conservation*, chapter Nasal-Emission and Nose leaves, page 22. Springer Science+Business Media, New York, N.Y., 2013.

[15] Gao L, Balakrishnan S, He W, Yan Z, and Müller R. Ear deformations give bats a physical mechanism for fast adaptation of ultrasonic beam patterns. *Phys. Rev. Lett.*, 107:214301, Nov 2011.

[16] Feng L, Gao L, Lu H, and Müller R. Noseleaf dynamics during pulse emission in horseshoe bats. *PloS ONE*, 7(5):e34685, 2012.

[17] Csorba C, Ujhelyi P, and Thomas N. *Horseshoe Bats of the World*. Alana Books, Bishop's Castle, Shropshire, UK, 2003.

[18] Kuc R. Morphology suggests noseleaf and pinnae cooperate to enhance bat echolocation. *J. Acoust. Soc. Am.*, 128:3190, 2010.

[19] Schneider H and Möhres F P. Die Ohrbewegungen der Hufeisenfledermäuse (Chiroptera, Rhinolophidae) und der Mechanismus des Bildhörens. *J. Comp. Physiol A*, 44(1):1–40, 1960.

[20] Mogdans J, Ostwald J, and Schnitzler H U. The role of pinna movement for the localization of vertical and horizontal wire obstacles in the greater horseshoe bat, *Rhinolophus ferrumequinum*. *J. Acoust. Soc. Am.*, 84:1676–1679, 1988.

[21] Walker V A, Peremans H, and Hallam J C T. One tone, two ears, three dimensions: A robotic investigation of pinnae movements used by rhinolophid and hipposiderid bats. *J. Acoust. Soc. Am.*, 104:569, 1998.

[22] Balakrishnan S. An numerical elastic model for deforming bat pinnae. Master's thesis, Virginia Polytechnic Institute and State University, 2010.

[23] Balakrishnan S, Gao L, He W, and Müller R. A digital model for the deformation of bat ears. *J. Acoust. Soc. Am.*, 127(3):1862–1862, 2010.

[24] Gao L, He W, Balakrishnan S, and Müller R. Ear deformations in the biosonar system of horseshoe bats. *J. Acoust. Soc. Am.*, 127:1861, 2010.

[25] Pannala M, Meymand S Z, and Müller R. Interplay of static and dynamic features in biomimetic smart ears. *Bioinspir. Biomim.*, 8(2):026008, 2013.

[26] Fletcher N H. *Acoustic systems in biology*. Oxford University Press, Oxford, 1992.

[27] Fletcher N H and Thwaites S. Obliquely truncated simple horns: idealized models for vertebrate pinnae. *Acta Acust/Acustica*, 65(4):194–204, 1988.

[28] Li G, Jones G, Rossiter S J, Chen S F, Parsons S, and Zhang S. Phylogenetics of small horseshoe bats from east asia based on mitochondrial dna sequence variation. *J. Mammal.*, 87(6):1234–1240, 2006.

[29] Jones G and Rayner J M V. Foraging behavior and echolocation of wild horseshoe bats *Rhinolophus ferrumequinum* and *R. hipposideros* (chiroptera, rhinolophidae). *Behav. Ecol. Sociobiol.*, 25(3):183–191, 1989.

[30] Lawrence B D and Simmons J A. Echolocation in bats: The external ear and perception of the vertical positions of targets. *Science*, 218(4571):481–483, 1982.

[31] Müller R. A numerical study of the role of the tragus in the big brown bat. *J. Acoust. Soc. Am.*, 116:3701–3712, 2004.

[32] Wotton J M, Haresign T, and Simmons J A. Spatially dependent acoustic cues generated by the external ear of the big brown bat, *Eptesicus fuscus*. *J. Acoust. Soc. Am.*, 98:1423–1445, 1995.

[33] Wotton J M, Haresign T, Ferragamo M J, and Simmons J A. Sound source elevation and external ear cues influence the discrimination of spectral notches by the big brown bat, *Eptesicus fuscus*. *J. Acoust. Soc. Am.*, 100:1764–1776, 1996.

[34] Müller R, Lu H, and Buck J R. Sound-diffracting flap in the ear of a bat generates spatial information. *Phys. Rev. Lett.*, 100:108701, Mar 2008.

[35] Kuc R. Model predicts bat pinna ridges focus high frequencies to form narrow sensitivity beams. *J. Acoust. Soc. Am.*, 125:3454, 2009.

[36] Zhuang Q and Müller R. Noseleaf furrows in a horseshoe bat act as resonance cavities shaping the biosonar beam. *Phys. Rev. Lett.*, 97(21):218701, 2006.

[37] Zhuang Q and Müller R. Numerical study of the effect of the noseleaf on biosonar beamforming in a horseshoe bat. *Phys. Rev. E*, 76(5):051902, 2007.

[38] Zhang Z, Truong S N, and Müller R. Acoustic effects accurately predict an extreme case of biological morphology. *Phys. Rev. Lett.*, 103(3):038701, 2009.

[39] Müller R, Pannala M, Reddy O P K, and Meymand S Z. Design of a dynamic sensor inspired by bat ears. *Smart Mater. Struct.*, 21(9):094025, 2012.

[40] Meymand S Z, Pannala M, and Müller R. Characterization of the time-variant behavior of a biomimetic beamforming baffle. *J. Acoust. Soc. Am.*, 133:1141–1150, 2013.

[41] Jen P H-S. Adaptive mechanisms underlying the bat biosonar behavior. *Front. Biol.*, 5(2):128–155, 2010.

[42] Suga N. Biosonar and neural computation in bats. *Sci. Am.*, 262(6):60–68, 1990.

[43] Müller R and Kuc R. Biosonar-inspired technology: goals, challenges and insights. *Bioinspir. Biomim.*, 2(4):S146, 2007.

[44] Cover T and Thomas J. *Elements of Information Theory*. Wiley Series in Telecommunications. John Wiley & Sons, Inc., 1991.

[45] Rieke F, Warland D, de Ruyter von Stevenick R R, and Bialek W. *Spikes*. The MIT Press, Cambridge, Massachusetts, 1996.

[46] Alexander Borst and Frédéric E Theunissen. Information theory and neural coding. *Nature neuroscience*, 2(11):947–957, 1999.

[47] Quiroga R Q and Panzeri S. Extracting information from neuronal populations: information theory and decoding approaches. *Nat. Rev. Neurosci.*, 10(3):173–185, 2009.

[48] Strong S P, Koberle R, de Ruyter van Steveninck R R, and Bialek W. Entropy and information in neural spike trains. *Phys. Rev. Lett.*, 80(1):197, 1998.

[49] Chase S M and Young E D. Cues for sound localization are encoded in multiple aspects of spike trains in the inferior colliculus. *J. Neurophysiol*, 99(4):1672–1682, 2008.

[50] Shew W L, Yang H, Yu S, Roy R, and Plenz D. Information capacity and transmission are maximized in balanced cortical networks with neuronal avalanches. *J. Neurosci.*, 31(1):55–63, 2011.

[51] Steuer R, Kurths J, Daub C O, Weise J, and Selbig J. The mutual information: detecting and evaluating dependencies between variables. *Bioinformatics*, 18(suppl 2):S231–S240, 2002.

[52] Studholme C, Hill D L G, and Hawkes D J. An overlap invariant entropy measure of 3d medical image alignment. *Pattern Recogn.*, 32(1):71–86, 1999.

[53] Suzuki R, Buck J R, and Tyack P L. Information entropy of humpback whale songs. *J. Acoust. Soc. Am.*, 119:1849, 2006.

[54] Vinh N X, Epps J, and Bailey J. Information theoretic measures for clusterings comparison: Variants, properties, normalization and correction for chance. *J. Mach. Learn. Res.*, 9999:2837–2854, 2010.

[55] Reijniers J, Vanderelst D, and Peremans H. Morphology-induced information transfer in bat sonar. *Phys. Rev. Lett.*, 105(14):148701, 2010.

[56] Summers J E. Information-theoretic performance analysis of azimuthal localization for spatial-auditory display of beamformed sonar data. In *Proceedings of the 16th International Conference on Auditory Display (ICAD), Washington, DC (June 9–15, 2010)*, 2010.

[57] Nemenman I, Lewen G D, Bialek W, and de Ruyter van Steveninck R R. Neural coding of natural stimuli: information at sub-millisecond resolution. *PLoS Comput. Biol.*, 4(3):e1000025, 2008.

[58] Shannon C E. A mathematical theory of communication. *Bell Syst. Tech. J.*, 27:379–423, 1948.

[59] Von Luxburg U. A tutorial on spectral clustering. *Stat. Comput.*, 17(4):395–416, 2007.

[60] Panzeri S, Senatore R, Montemurro M A, and Petersen R S. Correcting for the sampling bias problem in spike train information measures. *J. Neurophysiol.*, 98(3):1064–1072, 2007.

[61] Roulston M S. Estimating the errors on measured entropy and mutual information. *Physica D*, 125(3):285–294, 1999.

[62] Basharin G P. On a statistical estimate for the entropy of a sequence of independent random variables. *Theor. Probab. Appl+*, 4(3):333–336, 1959.

[63] Panzeri S and Treves A. Analytical estimates of limited sampling biases in different information measures. *Network-Comp. Neural.*, 7:87–107, 1996.

[64] Nelken I and Chechik G. Information theory in auditory research. *Hearing Res.*, 229(1):94–105, 2007.

[65] Hacine-Gharbi A, Deriche M, Ravier P, Harba R, and Mohamadi T. A new histogram-based estimation technique of entropy and mutual information using mean squared error minimization. *Comput. Electr. Eng.*, 2013.

[66] Press W H, Teukolsky S A, Vetterling W T, and Flannery B P. *Numerical Recipes in C: The Art of Scientific Computing*. Cambridge University Press, 2nd edition, 1992.

[67] Schneider H. Die Ohrmuskulatur von *Asellia tridens* Geoffr. (Hipposideridae) und *Myotis myotis* Borkh. (Vespertilionidae) (Chiroptera). *Zool. Jahrb. Allg. Zool.*, 79:93–122, 1961.

[68] Göbbel L. The external nasal cartilages in chiroptera: significance for intraordinal relationships. *J. Mamm. Evol.*, 7(3):167–201, 2000.

Chapter 7

Appendix A

Binning effect on a Gaussian distribution:

Consider a Gaussian distribution with zero mean and standard deviation of 1. The distribution was binned with sizes ranging from 2 to 10000 (s. Figure 7.1).

Numbers of bins that are too small (e.g., Size=2 in Figure 7.1) do not represent the Gaussian distribution, because important features are lost. If the number of bins is too high (e.g., Size=10,000 in Figure 7.1), again an incorrect picture of distribution is the result, because the true distribution is reduced to a set of spikes at bins that happen to contain a single sample. Hence, an optimum bin size needs to be found that represents the features of the distribution without degenerating into single spikes.

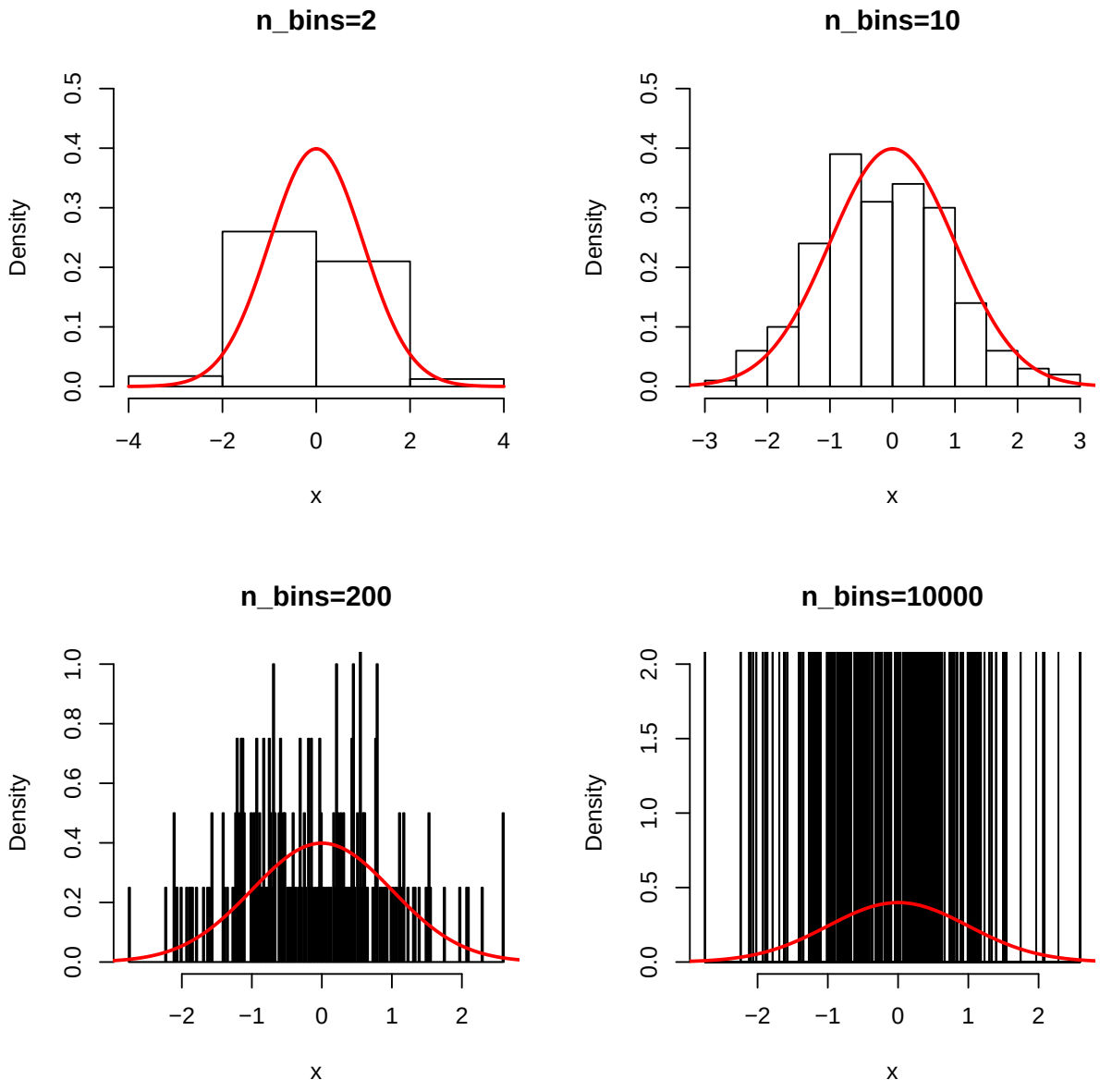

Figure 7.1: Gaussian distribution binned with bin numbers of 2, 10, 200, and 10,000. The continuous distribution is represented by the red line.

Chapter 8

Appendix B

Mutual Information for two Gaussian variables:

Consider two continuous variables with Gaussian distribution of mean 0 and standard deviation 1.

By calculating the marginal and joint probability density functions, exact values of mutual information can be found.

Discrete values of variables with normal random distribution can be found for alphabet sizes ranging from 1 to 100.

By applying the permutation tests, the Mutual Information between the two Gaussian variables increases to a maximum and then decays to zero.

Such tests were performed for correlation values varying from 0 to 0.95 between the two Gaussian variables (s. Figure 8.1).

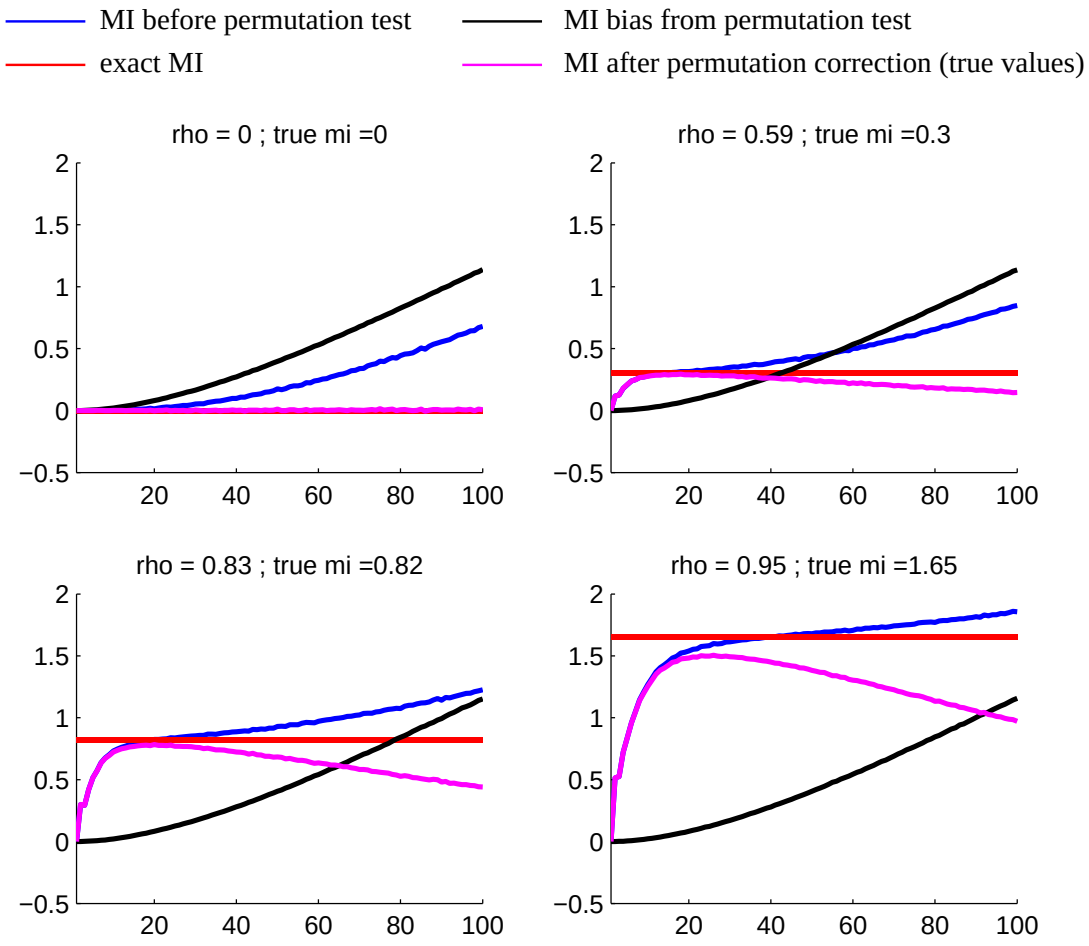

Figure 8.1: True mutual information evaluated from the permutation tests.